



---

**Petrological and Geochemical Characteristics of Wadi Sikait Lamprophyre Dykes, South Eastern Desert, Egypt: Implications for Petrogenesis and Crustal Contamination**

**Amira M. El Tohamy, Mohamed S. Kamar and Ahmed M. Ismail**

Nuclear Materials Authority, P.O. Box 530 El Maadi, Cairo, Egypt

**Received:** 15 Mar. 2023

**Accepted:** 20 April 2023

**Published:** 10 May 2023

---

**ABSTRACT**

The lamprophyre dykes extruded in the psammitic gneisses, ophiolitic mélange, and monzogranites at Wadi Sikait provinces. Microscopic investigation of the lamprophyres indicates that they are mostly composed of spessartites and kersantite. The microscopic and ESEM investigations on the accessory minerals revealed the presence of monazite-allanite, yttracolumbite, gold, cassiterite, wolframite, galena, and native nickel. Geochemically, the lamprophyres are basalt and basanite/tephrite in composition with calc-alkaline characters. They are enriched in TiO<sub>2</sub>, Fe<sub>2</sub>O<sub>3</sub>, MnO, CaO, Na<sub>2</sub>O, P<sub>2</sub>O<sub>5</sub>, V, Zn, Li, Nb, Ta, Th, Zr, and U however depleted in SiO<sub>2</sub>, Al<sub>2</sub>O<sub>3</sub>, MgO, K<sub>2</sub>O, Cr, Co as well as Ni relative to the corresponding rock types. The high LILE contents, Nb and Ta relative to Hf, depletion in HREEs, along with elevated Ba/Nb and Ba/La ratio illustrate an enriched mantle source. The enrichment of LREEs in the lamprophyre dykes indicates a low degree of partial melting. High Ba and U values implies the addition of Ba and U to the protolith via metasomatism or hydrothermal fluids in the source region. The peculiar M-W type tetrad effect confirms the effect of the water-rich phase and could be an indication of Au mineralization, as indicated by the presence of gold grains in the separated heavy fraction.

**Keywords:** Lamprophyre dyke, Gold, Base metals, REEs, Eastern Desert, Egypt

---

**1. Introduction**

Lamprophyres, a type of melanocratic hypabyssal igneous rock distinguished by microporphyritic textures and mafic phenocrysts (Rock, 1991), are found in a variety of tectonic settings (Madhavan *et al.*, 1998) and are thought to have close temporal-spatial relationships to gold mineralization in some large- and super-large-sized gold districts (Huang *et al.*, 2002). Their petrogenesis is complex and diverse, and they are generally classified into three models: (1) partial melting of metasomatic lithospheric mantle (Zhang *et al.*, 2003), either in a subduction related environment (Huang *et al.*, 2002) or in the sub-continental lithospheric mantle (Fowler and Henney, 1996); (2) continental crust contamination of mafic magmas (Currie and Williams, 1993); or (3) mixing of upwelling basaltic magma with various proportions of ultrapotassic lithospheric-mantle melts (Thompson *et al.*, 1990), or of mantle-derived basaltic or lamproite melts and crustal derived silica melts (Prelevic *et al.*, 2004). Lamprophyres are classified into five groups (Le Maitre, 1989; Rock, 1991). These are (i) calc-alkaline lamprophyres (CAL); ii) alkaline lamprophyres (AL), iii) ultramafic lamprophyres (UML), iv) lamproitic lamprophyres (LL), and v) kimberlitic lamprophyres. The calc-alkaline types are commonly found in convergent tectonic environments and are thought to form from volatile-rich, crystal-laden fluids, whereas the alkaline and ultramafic types are found in anorogenic extensional and divergent tectonic environments.

Lamprophyric melts provide information on their mantle source and geodynamic setting (e.g., Tappe *et al.*, 2006; Jiang *et al.*, 2010). It is generally believed that lamprophyre originates from mantle-derived magma (Rock, 1987; Foley, 1992) that itself had formed from partial melting of a phlogopite-

and/or amphibole-bearing lherzolite in the spinel-garnet transition zone (e.g., Rock, 1987; McKenzie, 1989).

Lamprophyre dykes are generally thought to be good polymineralization traps (physical and chemical). Chemical traps include the transformation of feldspars to clay minerals, while physical traps include the transformation of pyrites and quartz leaves rounded to semi-circular vugs (box works).

The Nugrus – Sikait area covers about 320 km<sup>2</sup> and constitutes a part of the Arabian Nubian Shield bordering to the major shear zone known as Nugrus thrust fault (Greiling *et al.*, 1988), or Nugrus strike-slip fault (Fritz *et al.*, 1996) and Sha'it-Nugrus shear zone. This shear zone separates the Hafafit complex (high-temperature metamorphic rocks) in the SW from Ghadir group (mainly low-grade ophiolitic and arc volcanic assemblages), (Fowler and Osman, 2009). The Nugrus thrust runs along the upper part of Wadi (W.) Sikait in NW direction till the southern tip of G. Ras Sha'it, then swings to a south westward direction along W. Sha'it west of G. Migif. The Migif-Hafafit gneisses represent the foot wall of the Nugrus thrust, while the Ghadir group represents the hanging wall (El Bayoumi, 1980).

W. Sikait area is located about 95 km southwest of Marsa Alam City in the south Eastern Desert (ED) of Egypt. This area is one of the most promising areas in the Eastern Desert. Archaeologically, there is Sikait temple in the middle of the wadi, which considers a tourist attraction. There are abundant old workings of beryl and emerald that occurs in parts of W. Sikait and Gabel (G.) Sikait. There is also paragneiss that occurs in the middle part of W. Sikait, which contains radioactive minerals like thorite, uranothorite, and base metals. In the northern part of the wadi, metamorphosed sandstone existed in two parts and has a high concentration of uranium and molybdenum. W. Abu Rusheid lies in the west of W. Sikait and Sikait- Abu Rusheid pluton is elongated in NW-SE (12 km long) and thinning in NE-SW (3 km in width).

The previous works on the W. Sikait area are numerous (e.g., Ibrahim and Ragab, 2011; Saleh *et al.*, 2012; Ibrahim, 2013, El Tohamy, 2019 and Kamar *et al.*, 2022). The type of W. Sikait lamprophyres was not achieved.

Therefore, this paper will shed light on the petrographic classification of lamprophyre for the first time, base metal and radioactive mineralization, in addition to the geochemical characteristics of the lamprophyre dykes at the study area.

## 2. Geologic setting

The study area lies between latitudes 24° 38' 20" to 24° 39' 20" N and longitudes 34° 47' 03" to 34° 48' 06" E (Fig. 1a). The tectono-stratigraphic sequence begins from the oldest to youngest as follows; psammitic gneisses, ophiolitic mélange, monzogranite, and lamprophyre dykes.

The psammitic gneiss formed an elongated zone striking NNE-SSW at the contact with the ophiolitic mélange from the eastern and western sides of W. Sikait (Fig. 1b) cutting by right-lateral strike-slip faults. There is a sharp contact with the monzogranites from the western and northern parts of the mapped area. The rock is reddish in color, fine- to medium- grained, low to moderate topographic terrains and down thrusts the ophiolitic mélange (Fig. 2a). The rock is jointed, sheared, mylonitized, hematized and banded with dipping 48°-68° to NNW direction.

The ophiolitic mélange represents the hanging wall of the major thrust in the study area and thrusts over the gneissic rocks. It comprises a metamorphosed sedimentary matrix (biotite–phlogopite schist, garnetiferous hornblende biotite schist, and garnetiferous staurolite schist) enclosing serpentinite, metagabbros and orthoamphibolite fragments mounted in schists (Saleh, 1997). Monzogranite is characterized by pinkish-gray and coarse-grained K-feldspar crystals up to 2 cm in length. Monzogranite is fractured and exfoliated as well as deformed and has gneissose structures along the contact with the oldest rocks. Sometimes, monzogranite is highly fractured and hematized with high radioactive measurements especially along the fault plane of a right lateral strike-slip fault (Kamar, 2021).

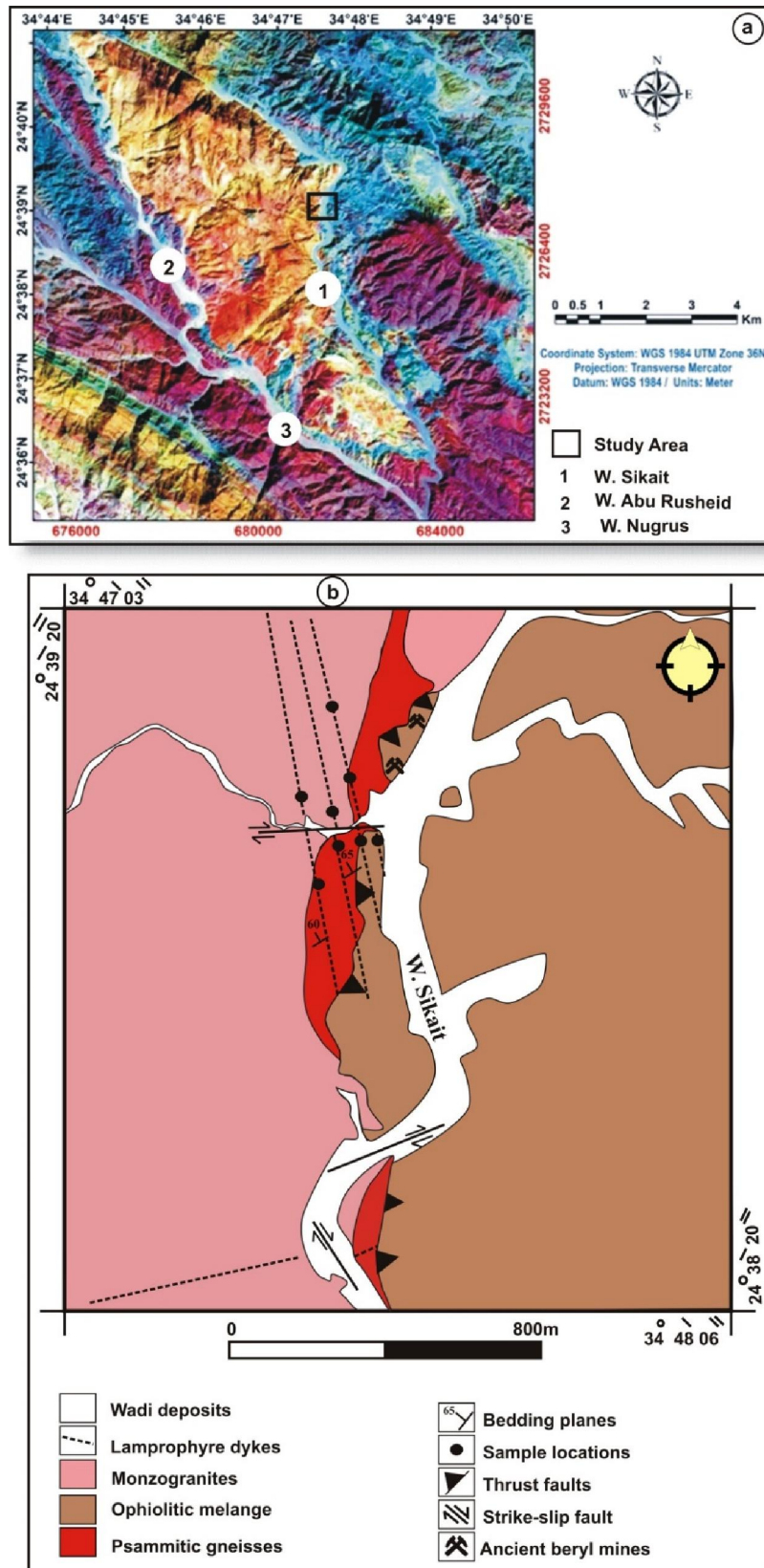


Fig. 1. a: Landsat image showing the location of the study area. b. Geological map of W. Sikait, SED, Egypt (modified after Kamar *et al.*, 2022).

Lamprophyre dykes as well as the mineralized occurrences could be formed at the transition stage of the regional structural stress field from compression to extension and can be used to mark the ending of a deformational shortening-extension cycle (Ibrahim *et al.*, 2015). The lamprophyre dykes range from 0.5–1.5 m in width, 0.1–1.0 km in length. These lamprophyre dykes are characterized by variable colors (black, pink, and red) depending on the degree of alterations (kaolinitization, ferrugination, carbonitization, fluoritization, hematitization and sericitization). These dykes are almost vertical dip strikes NNW-SSE and ENE-WSW intrudes the psammitic gneiss, ophiolitic mélangé and monzogranite and cut by right lateral strike slip faults (Fig. 2b).

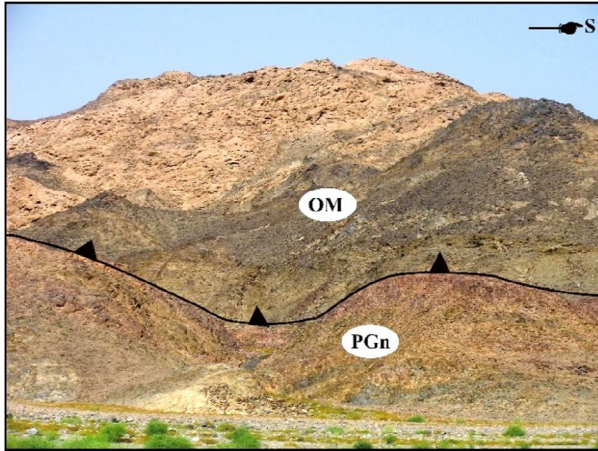


Fig. 2a: Elongated zone of psammitic gneiss (PGn) down thrusted by ophiolitic mélangé (OM), W. Sikait, SED, Egypt.



Fig. 2b: Lamprophyre dyke cut psammitic gneisses (PGn), and then cut by right strike slip fault, W. Sikait, SED, Egypt.

### 3. Materials and Methods

A total of 8 representative samples were collected from the Sikait- lamprophyre dyke. Each sample was crushed, ground, quartered, and sieved. The size fraction 0.125–0.250 mm was washed, and its heavy fraction was separated using bromoform and subjected to magnetic fractionation using Frantz Isodynamic Magnetic Separator (Model LB 1). The intended minerals were picked using the binocular microscope to obtain mono-mineralic fractions for identification and analysis. Mineral identification was achieved using the environmental scanning electron microscope (ESEM model Philips XL 30) supported by an energy dispersive spectrometer (EDX) unit. The concentrations of major oxides, trace, and rare earth elements in the bulk samples were determined using inductively coupled plasma-mass spectrometry (ICP-MS) at the ACME Analytical Laboratories LDT, Canada. Major oxide concentrations and trace elements/rare earth are indicated by weight (% by weight) and parts per million (ppm), respectively. Major oxide detection limits ranged from 0.001 weight percent to 0.04 weight percent, and trace element detection limits ranged from 0.01 to 0.5 ppm. Analytical precision, as determined by replicate analyses, ranged from 2 % to 20 % for trace elements and was 0.5 % for major elements. 1 gramme of each sample was heated at 950° C for 90 minutes in order to determine the loss on ignition (L.O.I).

### 4. Result and Discussion

#### 4.1. Petrographic study

Lamprophyres are rocks that contain phenocrysts of biotite, amphibole, and pyroxene. They vary from porphyries and porphyrites, which have two generations of feldspar crystallization. Dyke rocks, as well as peripheral facies of plutonic intrusions, are mainly found as dykes and sills. Due to the prevalence of ferro-magnesian silicates, they are often black in colour, have a high specific gravity and prone to decomposition.

So, they are classified as a melanocratic series (rich in dark minerals), frequently accompanied by a complementary leucocratic series (rich in the white minerals feldspar and quartz). The species are determined by the presence or lack of the four major minerals orthoclase, plagioclase, biotite, and hornblende:

- Minette contains biotite and orthoclase.
- Kersantite contains biotite and plagioclase.
- Vegemite contains hornblende and orthoclase.
- Spessartite contains hornblende and plagioclase.

Megascopically, the lamprophyre samples are predominantly melanocratic rock, with inequigranular, holocrystalline panidiomorphic texture in hand specimens.

Microscopic investigation of the lamprophyres of W. Sikait area indicates that they are mostly spessartites and kersantite.

### I-Spessartites

Spessartites contain phenocrysts of brown amphibole, plagioclase, and carbonate mineral (calcite), embedded in fine grained groundmass. Opaques, apatite, antigorite and quartz are accessories. Brown amphibole minerals (hornblende, actinolite) are subhedral–anhedral, constitutes up to 40% of the phenocrysts, occurring as elongated crystals up to 5 mm. Plagioclase (2–5%) embedded in a fine grained microcrystalline groundmass (57–85 %), consisting of the same constituents. Antigorite occurs as euhedral to subhedral serpentinites mineral and surrounded by carbonate. Apatite occurs as anhedral crystal with sub-rounded shape, usually found as minute six-sided prismatic crystals, with moderate relief and weak birefringence (Fig. 3 a -d).

### II-Kersantite

Biotite occurs as flakes showing strong pleochroism from brown to deep brown color (Fig. 3e & f). Plagioclase occurs as euhedral crystals showing Carlsbad twinning with corroded boundaries (Fig. 3g). Calcite is distinguished by its high order, often disallowed color and rhombahedral twinning (Fig. 3h). The lamprophyre calcite is magmatic (primary) based on the petrographic intergrowths of calcite ocelli and other minerals observed in thin section. Apatite founded as fine elongated crystals. Opaques occur as irregular interstitial grains or as inclusions within the ferromagnesian minerals.

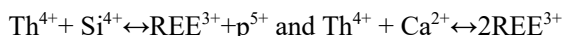
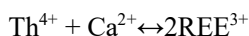
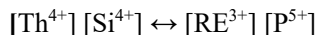
## 4.2. Mineralogical investigations

A combination of binocular microscope, scanning electron microscope (ESEM/EDX) and back-scattered electron imaging (BSE) analysis of heavy minerals associated with Sikait lamprophyre dyke revealed the dominance of diversified mineral assemblages that include radioactive, Nb-Ta, rare earth minerals and base metals (Table 1).

### 4.2.1. Monazite- Allanite solid solution

So far, two major alteration processes and products for monazite have been identified: (i) Monazite-fluid ion exchange (REE, Ca, Y, Th, U) occurs along fissures and the mineral's periphery without causing significant disruption to the [PO<sub>4</sub>] sub-lattice, and (ii) complete mineral breakdown occurs, resulting primarily in apatite + allanite mineral assemblage. The obtained mineral assemblages show that during the monazite alteration in post-magmatic conditions can be actually considered as a residue after the alteration, while the well crystalline mineral forms (thorite) as mobilized and precipitated components of the monazite.

The alteration of monazite is possible already by subsolidus magmatic fluids in low-temperature conditions. In such conditions, monazite breaks down and newly-formed LREE enriched apatite forms on the monazite grains. Thorium is usually present in monazite substituting for the rare earth from a few percent up to at least 27 wt.% (Fron del, 1958). Silicon can substitute for P in amounts up to 3 wt.% (Fron del, 1958). The fact that both Th, Si, REE, and P differ markedly from 1: 1 indicates the simple coupled substitution



Morin (1977) proposed a rather unusual scheme of coupled substitution:  $\text{REE}^{3+} + \text{Ca}^{2+} \leftrightarrow \text{Al}^{3+} + (\text{Fe}^{3+}, \text{Fe}^{2+})$  for allanite from granitic rocks.

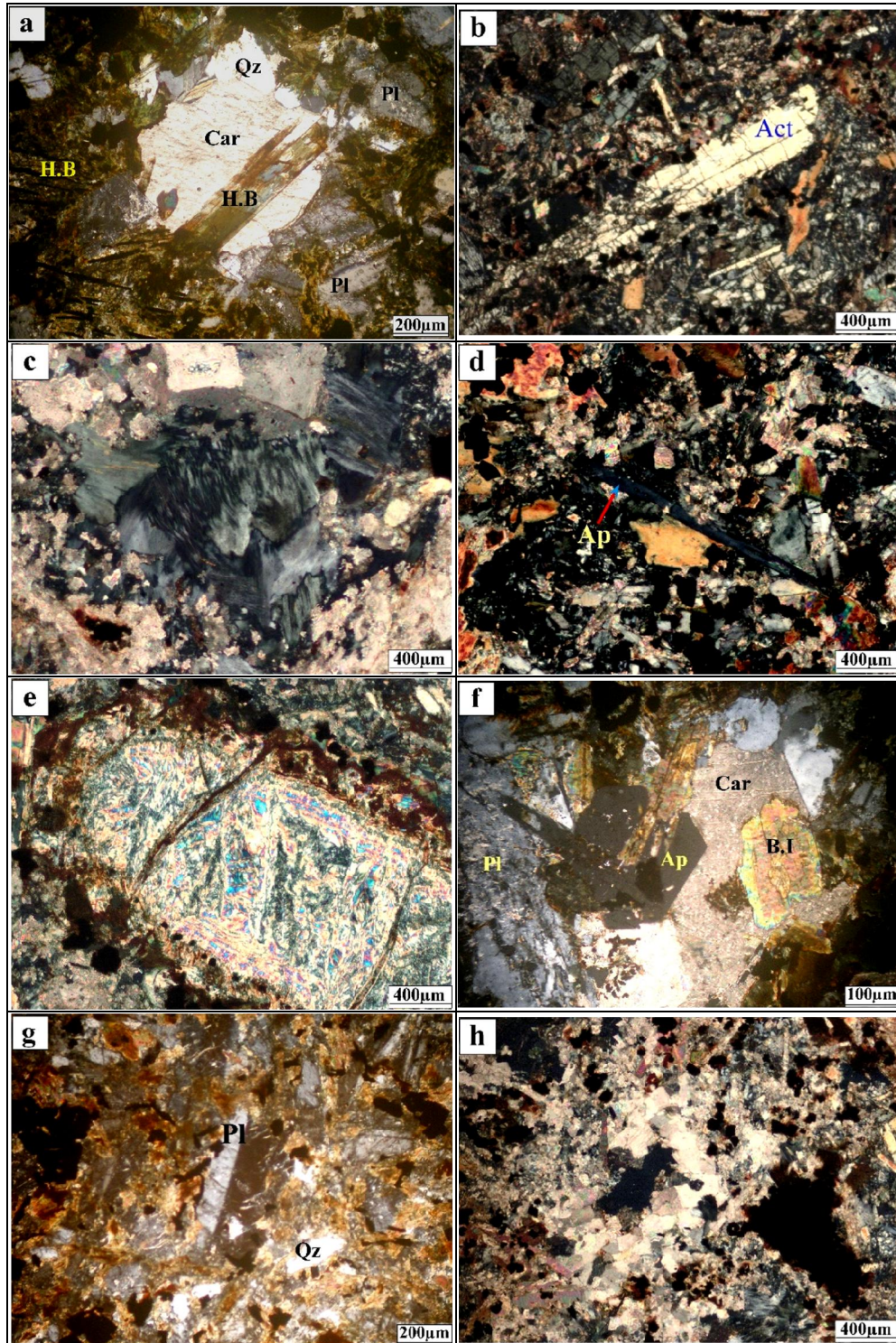


**Fig. 3: Photomicrographs of lamprophyre dykes showing:**

a) Anhedral crystal of biotite (H.B.) associated with carbonate, (C.N.). b) Subhedral crystal of actinolite (Act), (C.N.). c) Euhedral crystal of antigorite surrounded by carbonate, (C.N.). d) Elongated crystal of apatite, (Ap) (C.N.). e) Elongated crystal for pseudomorph of mica mineral, (C.N.). f) Broad crystal of biotite (B.I) associated with carbonates (Car) and apatite (Ap), (C.N.). g) Euhedral crystal of plagioclase (Pl) showing Carlsbad twinning, (C.N.). h) Euhedral crystals of carbonate, (C.N.).

Allanite-monzonite reactions are most likely connected to low-temperature hydrothermal changes. Also, alteration affects of Th-rich minerals (monazite and thorite) more than Th-poor phases. This could be the result of chemical disequilibrium at low temperatures or incomplete metamictization prior to modification (Berger *et al.*, 2008). The worm-like allanite is typically found in rocks that have been directly affected by late-post-magmatic hydrothermal alteration and is thought to be a clue to metamictization processes. (El-Balakssy *et al.*, 2012 & Ibrahim *et al.*, 2015). Kamar *et al.*, (2022) recorded the alteration of monazite to cheralite in the study area. The BSE image and EDX spectrum of Sikait lamprophyre samples illustrate the relation between monazite and allanite as shown in figure 4.

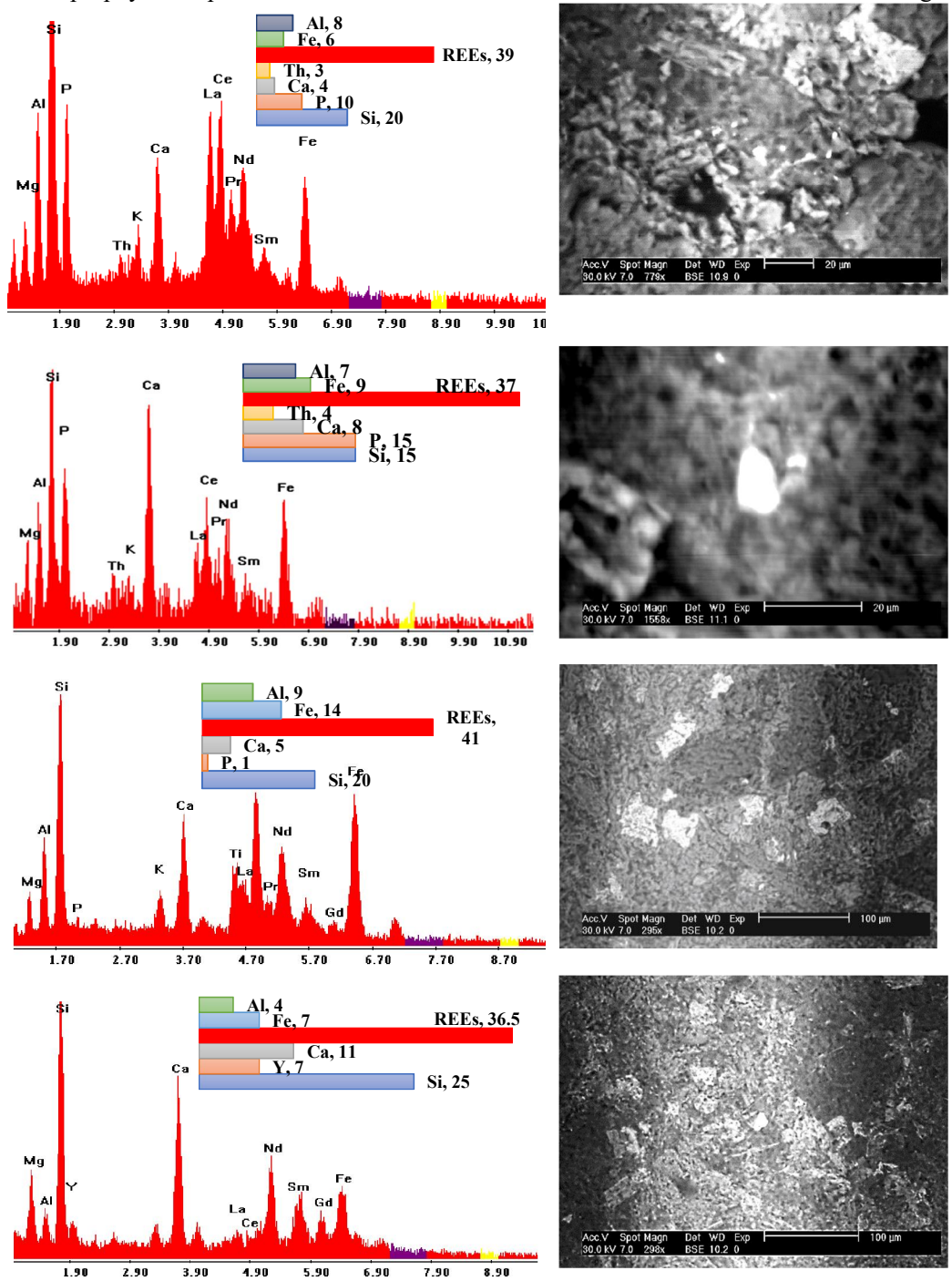


**Fig. 4:** EDX and BSE image showing monazite-allanite minerals, lamprophyre dyke, W. Sikait, SED, Egypt.

**3.2.2. Yttrocolumbite [(Y, U, Fe<sup>++</sup>) (Nb, Ta) O<sub>4</sub>]**, the name is derived from its yttrium content and similarity to columbite. It was confirmed by EDX analyses, which clarify that it is composed of Nb (40 wt. %), Y (9-13 wt. %), Ta (1 wt. %), Fe (14 wt. %) with traces of LREEs (Fig. 5).

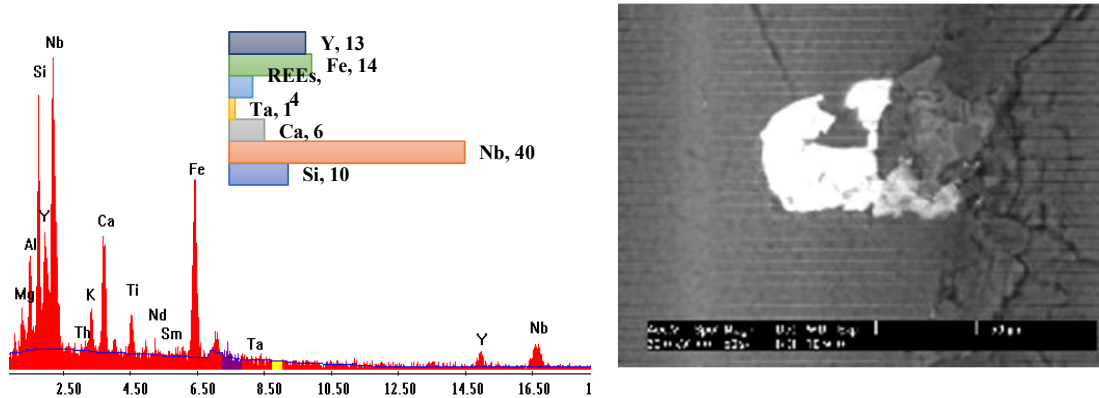
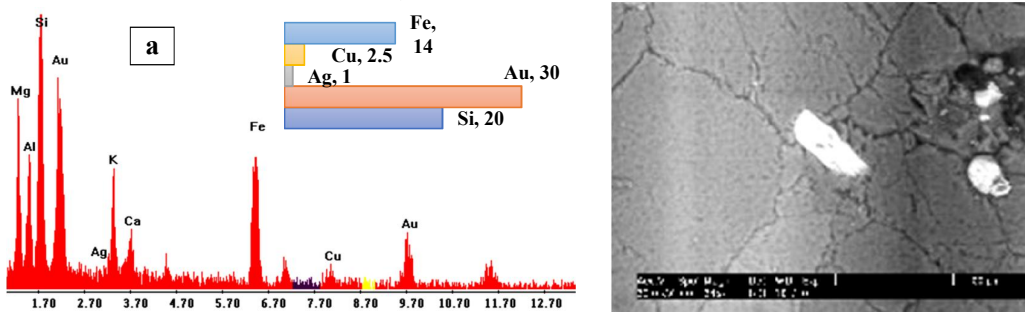
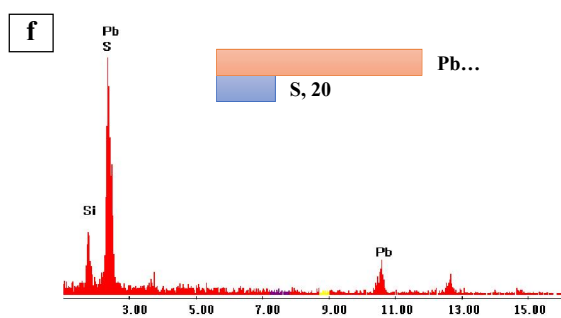
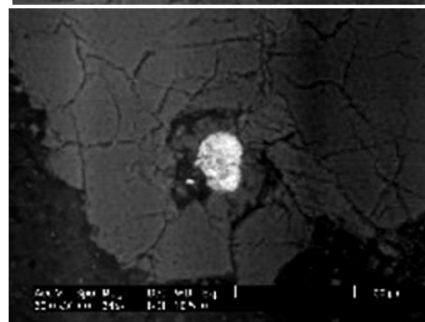
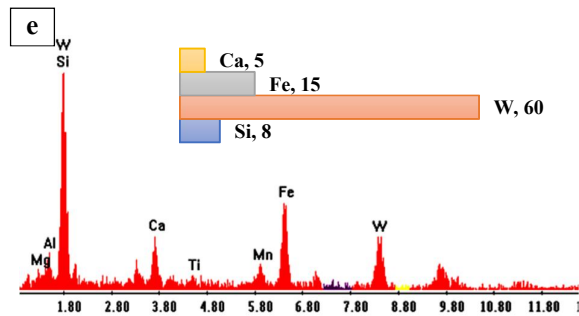
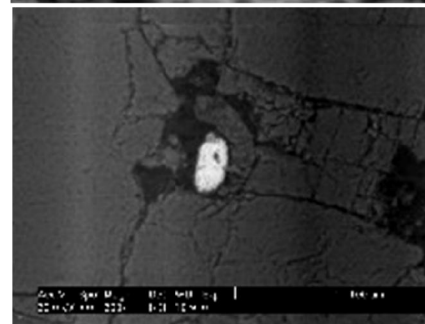
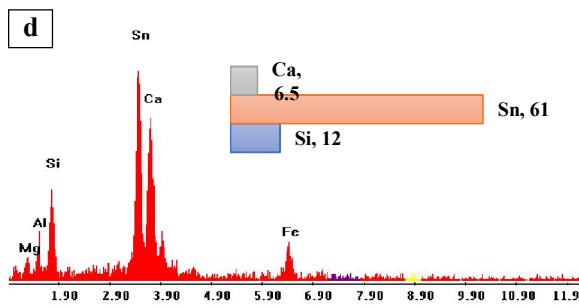
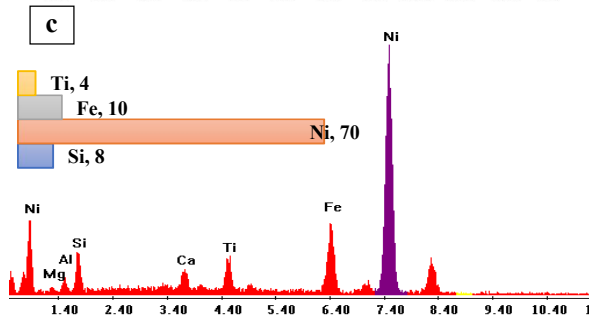
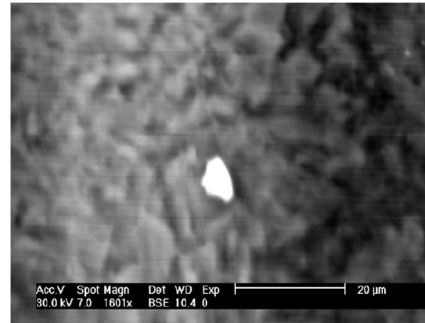
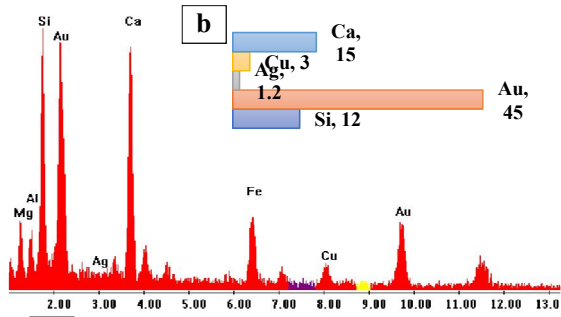


Fig. 5: EDX and BSE image showing yttrocolumbite mineral, lamprophyre dyke, W. Sikait, SED, Egypt.

#### 4.2.3. Base metals

Gold (Au) is the main precious metal recorded in the study area, occurs as fine crystals (~ 10-20 μm), having Au content range (30-45 wt. %), Ag (1-1.2 wt. %), Cu (2.5-3 wt. %) with minor amounts of Fe and Si as confirmed by EDX analyses (Fig. 6a & b). El Tohamy (2019) confirmed the presence of gold in the study area by fire assay and the estimated gold contents were 0.48 g/t to 0.52 g/t. The recorded specks of gold may be transported from the ophiolitic metagabbros. Native nickel (Ni) was found out and confirmed by EDX analyses, which show that Ni content reaches up to (70 wt. %), with traces of Si and Fe (Fig. 6c). Cassiterite (SnO<sub>2</sub>) belongs to rutile group. It is found in medium- to high-temperature hydrothermal veins. EDX analyses gave Sn content (61 wt. %), with traces of Ca, Si, and Al (Fig. 6d). Wolframite (Fe, Mn)WO<sub>4</sub> is an iron, manganese, and tungstate mineral that is intermediate between ferberite (Fe<sup>2+</sup> rich) and hübnerite (Mn<sup>2+</sup> rich). The wolframite series are the most important tungsten ore minerals. EDX analyses gave W content (60 wt. %) and Fe (15 wt. %), with traces of Ca and Mn (Fig. 6e). Galena (PbS) is the natural mineral form of lead (II) sulfide. It is the most important ore of lead and an important source of silver (Young *et al.*, 2008). Within the weathering or oxidation zone, galena altered to anglesite (lead sulfate) or cerussite (lead carbonate), (Da Silva, 2004). It contains high Pb (70 wt.%) and S (20 wt.%), (Fig. 6f).





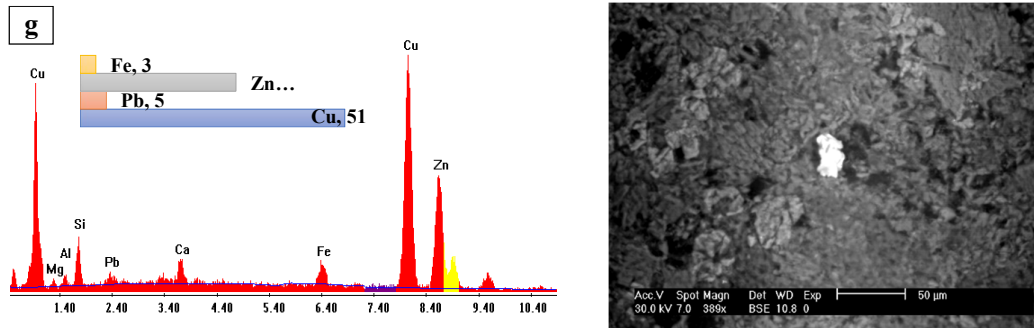


Fig. 6: BSE images and EDX patterns of (a & b) gold, (c) native nickel, (d) cassiterite, (e) wolframite, (f) galena, (g) brass alloy, lamprophyre dyke, W. Sikait, SED, Egypt.

Brass is an alloy of copper and zinc, in proportions that can be varied to achieve varying in mechanical, electrical, and chemical properties. It is a substitutional alloy: atoms of the two constituents may replace each other within the same crystal structure. It is mainly composed of Cu (51 wt.%), Zn (30 wt.%), and Pb (5 wt.%), (Fig. 6g).

**Table 1:** Semi-quantitative chemical composition and modes of occurrence of the identified heavy minerals in the studied rock.

Mineral & Chemical composition	SEM/EDX analysis (wt.%)	Form and Mode of occurrence
*Kasolite Pb (UO <sub>2</sub> ) (SiO <sub>4</sub> ). H <sub>2</sub> O	U (41), and Pb (36)	Scattered crystals on quartz surface (100 µm)
*Thorite (ThSiO <sub>4</sub> )	Th (52), U (8), and Si (14)	Minute aggregates on the surfaces of quartz
*Uranothorite (Th, U) SiO <sub>4</sub>	Th- (64) and U (15.5)	Minute aggregates on the surfaces of quartz
*Cheralite CaTh(PO <sub>4</sub> ) <sub>2</sub>	P (9-6), Th+U (50-40), Ca (5.5-4) and LREEs (15-9).	Subrounded grains and minute aggregates
Monazite- Allantite solid solution	Si (15-25), P (0-15), Ca (4-11), Th (0-4), REES (36-41), Fe (6-14)	Patches of solid solution between monazite and allantite on the surfaces of quartz crystals
Yttrocolumbite (Y, U, Fe <sup>++</sup> ) (Nb, Ta) O <sub>4</sub>	Nb (40), Y (13), Ta (1), Fe (14) with traces of LREEs.	Euhedral crystals
Gold Au	Au (45-30), Ag (1-1.2), Cu (2.5-3)	Fine crystals (~ 10-20 µm)
Native nickel Ni	Ni (70)	Minute angular grains
Cassiterite SnO <sub>2</sub>	Sn (61)	Elongated crystals
Wolframite Fe, Mn) WO <sub>4</sub>	W (60) and Fe (15)	Subhedral crystals
Galena PbS	Pb (70), S (20)	Anhedral crystals
*Pyrite FeS <sub>2</sub>	S (52), Fe (46)	Subangular grains
Brass alloy	Cu (51), Zn (30), Pb (5)	Subrounded crystals
*Xenotime YPO <sub>4</sub>	Y (25), P (22), HREEs (30)	Subangular grains on quartz surface
*Apatite Ca PO <sub>4</sub>	P (15), Ca (10), LREEs (30)	Subangular grains on iron surface
*Baddeleyite ZrO <sub>2</sub>	Zr (80), Hf (2), Si (7)	Anhedral crystal on quartz surfaces

\*Minerals recorded by Kamar *et al.* (2022) in the study area.

### 4.3. Geochemistry

#### 4.3.1. Geochemical Affinity, Petrochemical Character & Classification

##### 4.3.1. 1. The major oxides

The major oxides, trace, and rare earth elements (REEs) concentrations of the lamprophyre dykes are shown in Tables 2, 3 & 4. Geochemically, the samples are of ultrabasic character (SiO<sub>2</sub> = 44 wt. %) and highly potassic (2.4 wt. %). The Al<sub>2</sub>O<sub>3</sub>, TiO<sub>2</sub>, and CaO have an average of 12.3 wt. %, 2.9 wt. % and 10.6 wt. % respectively.

**Table 2:** Concentrations of major oxides (wt.%) in the lamprophyre dykes, W. Sikait, SED, Egypt.

Sample	1	2	3	4	5	6	7	8	Av.	Av.**	Rock (1991)
SiO <sub>2</sub>	45.66	44.15	42.34	43.5	44.5	43.33	45.5	44.8	44.22	49.14	51
TiO <sub>2</sub>	2.49	2.656	3.32	3.2	2.9	3.06	3.1	3.0	2.97	3.54	1.1
Al <sub>2</sub> O <sub>3</sub>	11.28	12.22	13.16	12.5	12.6	12.63	11.9	12.6	12.36	12.72	14
Fe <sub>2</sub> O <sub>3</sub>	14.77	14.91	15.62	13.5	15.3	14.68	15.2	14.8	14.85	15.78	8.2
MnO	0.301	0.302	0.279	0.3	0.3	0.29	0.3	0.3	0.30	0.22	0.13
MgO	6.93	6.6	7.01	7	6.9	6.87	6.9	6.5	6.84	3.11	7
CaO	10.98	10.84	10.43	10.5	10.7	10.59	10.6	10.3	10.61	6.77	7
Na <sub>2</sub> O	2.9	3.1	2.9	3.2	2.8	2.80	2.9	3.0	2.95	2.63	2.7
K <sub>2</sub> O	2	2.4	2.8	2.4	2.3	2.53	2.5	2.5	2.43	1.75	3.1
P <sub>2</sub> O <sub>5</sub>	0.687	0.824	1.145	1.1	1	1.02	1.1	0.9	0.97	2.16	0.6
L.O.I	1.2	0.9	0.95	0.9	0.9	0.92	0.9	1.1	0.97	1.09	2
Total	99.2	98.9	99.9	98.1	100.2	98.72	100.93	99.79	99.47	98.89	96.8
S	0.15	0.17	0.04	0.15	0.16	0.12	0.1	0.1	0.13	0.10	0.12

Av. Average of the present study; Av\*\*. (El Tohamy, 2019)

**Table 3:** Concentrations of trace elements (ppm) in the lamprophyre dykes, W. Sikait, SED, Egypt.

Sample	1	2	3	4	5	6	7	8	Av.	Av**	Rock (1991)	PM*
V	217	225	243	570	573	577	613	614	454	177	170	82
Cr	150	126	116	261	253	270	303	305	223	39	370	3011
Co	50	53	53	49	55	51	50	54	52	31	36	105
Ni	88	100	113	98	95	94	110	103	100	162	150	2108
Cu	70	100	65	51	44	59	57	56	63	78.5	43	28.5
Zn	150	577	274	370	555	447	330	230	367	324.5	88	48.5
Pb	90	182	44	255	378	150	260	166	191	267.5	13	0.12
Li	152	192	210	150	200	190	180	160	179	64.5	44	2.15
Cs	10	52	51	50	45	30	25	40	38	5.9	3	0.023
Cd	0.4	0.9	0.7	0.5	0.7	0.9	0.4	0.7	0.65	0.295	--	0.026
As	3	2	2.5	4	3.4	5.4	2.5	4.7	3.44	18.5	3	0.15
Sb	0.2	0.23	0.25	0.1	0.25	0.21	0.3	0.2	0.22	0.155	0.6	0.005
Sn	3.5	3.6	3.5	3	3.4	2.5	4	3.6	3.39	3.7	2	0.17
BI	0.2	0.1	0.2	0.1	0.3	0.2	0.2	0.3	0.20	0.305	--	--
Mo	8	7	7	5	7	8	5	8	7	2.7	2	0.06
W	2	2	2.5	2.4	2.6	3	3.5	5	3	0.715	2.7	0.024
Sc	17.2	18	17	15	17	16	17	20	17.5	25.5	20	17
Rb	111	190	235	156	151	141	196	206	173	107.5	--	0.64
Sr	1172	1261	1124	1319	1090	1283	1258	1315	1228	499.5	715	21.1
Ga	23	24	26	31	11	3	26	14	20	26	18	3.8
Ba	848	937	1283	1113	1102	1169	1166	1153	1096	1089.5	1050	6.9
Y	50	60	43	56	63	56	47	58	54	122	23	4.55
Zr	310	355	388	490	481	470	472	492	432	555	190	11.2
Hf	7	7	8.6	9	8	7.5	8.5	9	8	14.5	5.2	0.308
Nb	160	80	121	180	79	165	77	150	127	119	13	--
Ta	1.5	3	6	2.5	3	2.4	5	3.6	3	2.8	0.9	0.04
Th	13	14	15	11	15	17	20	16	15	11.6	9	0.08
U	15	16	5	15	14	19	8	14	13	25	3	0.021
Ag(ppb)	250	1000	234	25	500	450	100	650	401	--	--	--

PM\*= Primitive Mantle after (Sun & McDonough, 1989); (-) = not detected; Av. Average of the present study; Av\*\*. (El Tohamy, 2019)

**Table 4:** Concentrations of rare earth elements (ppm) in the lamprophyre dykes, W. Sikait, SED, Egypt.

Sample	1	2	3	4	5	6	7	8	Av.	Av**	Rock (1991)
La	105	114	122	115	130	118	121.3	119.8	118	74.5	53
Ce	190	202	212	250	230	221.3	228.3	223.1	220	167.5	110
Pr	24	31	25	30	32	28.7	28.9	29.3	29	24.5	11
Nd	80	96	90	95	100	93.7	94.7	94.9	93	105	56
Sm	15	19	16	16	15	17.0	16.0	16.6	16	23	10.5
Eu	4.4	4.5	5	4	4	4.5	4.4	4.4	4	7	3.1
Gd	11	15	13	15	12	14.3	13.6	13.9	13	22.5	11
Tb	1.8	2.7	2	2	2	2.2	2.1	2.2	2	4	1.1
Dy	9	15	10	12	13	12.3	11.8	12.5	12	19.5	3.7
Ho	1.7	3	1.5	3	2.5	2.5	2.4	2.5	2	4	0.9
Er	5	8	5	8	7	7.0	6.8	7.0	7	10.5	1.6
Tm	0.7	1.2	1	1.2	1.2	1.1	1.1	1.1	1	2	0.24
Yb	8	7.9	4	7	8	6.3	6.3	6.6	7	10	1.8
Lu	1	1.1	0.5	1	1.1	0.9	0.9	0.9	1	1.5	0.26
ΣLREE	418	467	470	510	511	483	494	488	480	402	244
ΣHREE	38	54	37	49	47	47	45	47	45	74	21
ΣREE	457	520	507	559	558	530	538	535	526	476	264
LREEs/HREEs	10.95	8.65	12.70	10.37	10.92	10.35	10.99	10.45	10.57	5.45	11.6
Ce/Ce*	0.89	0.80	0.90	0.997	0.84	0.89	0.90	0.88	0.89	0.92	1.07
Eu/Eu*	1.05	0.82	1.06	0.79	0.91	0.88	0.91	0.89	0.91	0.94	0.88
Lu/Yb	0.13	0.13	0.12	0.14	0.13	0.14	0.14	0.13	0.14	0.15	0.14
Th/La	0.12	0.12	0.12	0.10	0.12	0.14	0.16	0.13	0.13	0.16	0.17
T1	1.13	0.93	1.21	1.19	1.03	1.11	1.13	1.09	1.10	1.02	0.9
T3	1.31	1.18	1.31	1.09	1.01	1.19	1.14	1.15	1.17	1.01	0.7
T4	0.61	1.06	1.74	1.19	1.04	1.25	1.25	1.20	1.17	1.17	1.06
T1.3	1.22	1.05	1.26	1.14	1.02	1.15	1.14	1.12	1.14	1.02	0.79

Av. Average of the present study; Av\*\*. (El Tohamy, 2019)

As a whole, the major oxides concentrations of the lamprophyre samples are comparable with those shown by averages of worldwide alkaline lamprophyres (Rock, 1991). There is an enrichment in TiO<sub>2</sub>, Fe<sub>2</sub>O<sub>3</sub>, MnO, CaO, Na<sub>2</sub>O and P<sub>2</sub>O<sub>5</sub> and depletion in SiO<sub>2</sub>, Al<sub>2</sub>O<sub>3</sub>, MgO and K<sub>2</sub>O (Table 2). Whereas; the major oxides are comparable with W. Sikait lamprophyre dykes (south of the study area, El Tohamy, 2019), with slight enrichment in MnO, MgO, CaO, Na<sub>2</sub>O as well as K<sub>2</sub>O and depletion in SiO<sub>2</sub>, TiO<sub>2</sub>, Al<sub>2</sub>O<sub>3</sub>, Fe<sub>2</sub>O<sub>3</sub> and P<sub>2</sub>O<sub>5</sub> (Table 2).

The chemical classification and nomenclature of the studied lamprophyres on total alkalis versus silica diagram after Cox *et al.* (1979) revealed that all samples fall between basanite/tephrite and basalt fields (Fig. 7).

In the binary diagram of MgO versus SiO<sub>2</sub> (Lefebvre *et al.*, 2005), the lamprophyre samples plot in the calc-alkaline lamprophyre field, (Fig. 8 a). The lamprophyre affinity of the dykes is evident by plotting samples on the ternary diagram between MgO-K<sub>2</sub>O-Al<sub>2</sub>O<sub>3</sub> (Bergman, 1987), the samples are positioned in lamprophyre field (Fig. 8b).

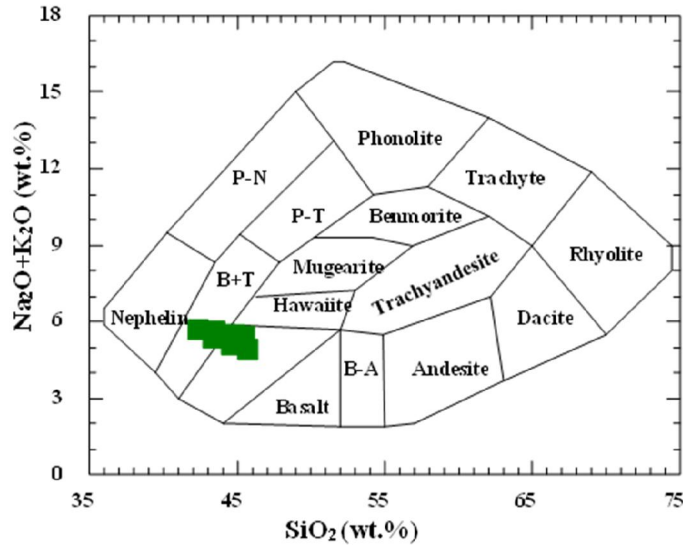


Fig. 7: Alkali oxides (wt.%) versus SiO<sub>2</sub> (wt.%) from Cox *et al.* (1979). B + T basanite and tephrites, P-T phonolitic tephrites, P-N phonolitic nephelinites.

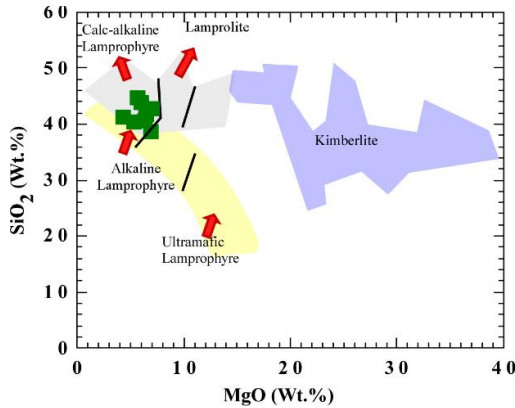


Fig. 8a: MgO- SiO<sub>2</sub> binary diagram showing the geochemical character of the lamprophyres, after Lefebvre *et al.* (2005).

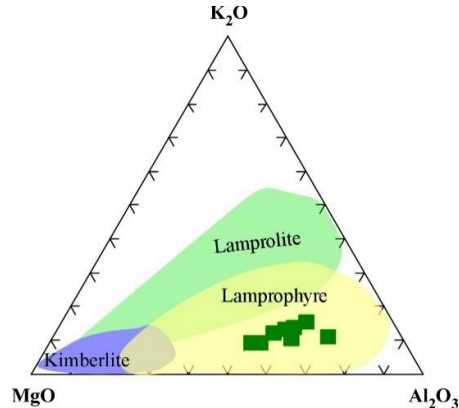


Fig. 8b: Plots showing the geochemical character of the lamprophyre dykes based on major element components, after Bergman (1987).

#### 4.3.1.2. Trace elements

##### a. Compatible elements

The compatible trace elements are comparable with those shown by averages of primitive mantle (PM) (Sun & McDonough, 1989). There is enrichment in V while other elements such as Cr, Co, and Ni are depleted (Table 3). This indicates that the source was either depleted in these elements or they were retained by compatible refractory phases during partial melting.

##### b. Incompatible elements

The incompatible element data were normalized using the PM values after McDonough & Sun, (1995) and plotted in Fig. (9). All the incompatible elements of the lamprophyre dyke are higher than those of the PM average (Table 3). This implies, the addition of Ba to the protolith via metasomatism or hydrothermal fluids in the source region. Ba/Rb and Rb/Sr ratios have been used as indices to ascertain the presence of amphiboles or biotite/phlogopite in the source region of the mantle.

An increase in Rb/Sr ratio value with respect to primitive mantle suggests the presence of phlogopite as the hydrous mineral in the source whereas high values of Ba/Rb confirms the presence of amphiboles (Furman and Graham, 1999). The elevated values of U indicate some forms of hydrothermal or crustal influence in the source or parental melts.

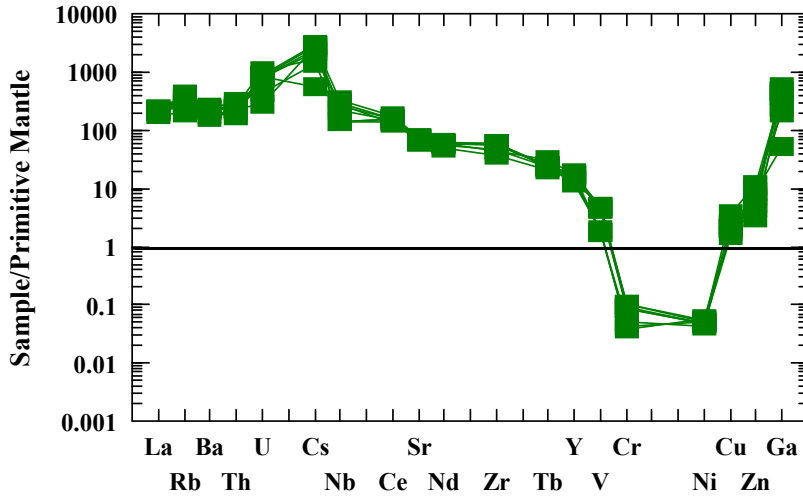


Fig. 9: Primitive-mantle normalized multi-element pattern for the lamprophyre samples (normalized after McDonough & Sun, 1995).

The high concentration of the LILE along with elevated Ba/Nb (Av. 7.7 ppm) and Ba/La (Av. 9.6 ppm), indicate an enriched mantle source of the lamprophyre (Ryan *et al.*, 1996; Kepezhinskas *et al.*, 2016).

However, the source of Ba could be also derived from a fluid source. Furthermore, the enrichment of Nb and Ta relative to Hf, coupled with small depletion in HREE elements in the lamprophyre samples when compared with lamprophyres of W. Sikait, could probably be explained by the enrichment in the upper mantle source (Pearce, 1983).

The Nb/Y versus Ba (Kepezhinskas *et al.*, 1997) diagram was used to analyze the involvement of slab associated melt or fluid enrichment of the source or protolith in the creation of these lamprophyres (Fig. 10). The data is shown along a fluid-related enrichment vector, implying that fluid melt-derived enrichment plays a role in the source region or protolith.

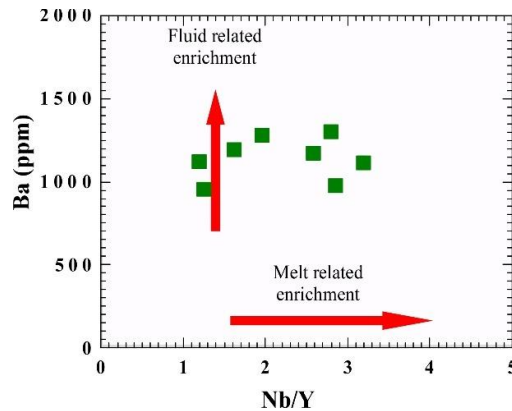


Fig. 10: Nb/Y – Ba plot of the sampled lamprophyres (after Kepezhinskas *et al.*, 1997).

#### 4.3.1.3. Rare earth elements (REEs)

In the most general terms, plagioclase-bearing lamprophyres (spessartites and camptonites) tend to have substantially lower Sm and Ce/Yb than plagioclase-free types (Rock, 1987) and total light rare earth elements (LREEs) increase with increasing K/Na and K-feldspar/plagioclase ratios (cf. Cullers & Graf, 1984).

The  $\Sigma$ REEs concentrations in the lamprophyre samples have an average of 526 ppm (Table 4). The average of LREE/HREE ratios are 10.57, this LREE enrichment is related mainly to the presence of monazite (cf. McLennan *et al.*, 1979).

The lamprophyre samples show coherent chondrite normalized REE patterns with LREEs enrichment (Fig. 11). The steeper HREE patterns with high LREE content indicate a low degree of partial melting. The low concentration of HREE suggests that garnet as a residue is under direct control (Le Roex *et al.*, 2003).

The REE profiles (Fig.11) show negative slopes above the C1 line (where LREE > HREE) following normalisation to C1 values (McDonough & Sun, 1995). The plotted profiles show a character derived from enriched source, residual garnet, and possibly high to moderate degrees of partial melting of the protolith. The Eu\* anomaly value (0.91) indicates that the protolith or source region was either lacking in Eu or plagioclase, or both.

The Eu anomaly may be due to REE mobility (Taylor and McLennan, 1980) or Eu leaching by the volatile phase (Taylor *et al.*, 1981). The Eu and Ce anomalies are very weak (Eu/Eu\* = 0.91 and Ce/Ce\* = 0.89, respectively), indicating that the melt doesn't have feldspar fractionation. The lamprophyre samples have an average Lu/Yb value of 0.15, indicating that the parental melts were produced from the mantle source (Sun and McDonough, 1989). The average La/Yb ratio is 18.3, but the average (La/Yb)<sub>N</sub> ratio is 11.8. These values are greater than one suggesting high LREE fractionated pattern, as well as residual/refractory garnet or garnet insufficiency in the protolith.

The tetrad effect is most commonly seen in the highly advanced silicate magmas and is caused by significant fluid-rock contact. In chondrite-normalized REE patterns, it becomes obvious. T1 = La-Nd, T2= (Pm) Sm- Gd, T3 = Gd-Ho, and T4= Er- Lu, all of which can be M- or W-shaped, according to Masuda *et al.* (1987). High water/rock ratios, pH, and numerous complexing ions CO<sub>3</sub><sup>2-</sup>, F<sup>-</sup>, Cl<sup>-</sup>, PO<sub>4</sub><sup>2-</sup>, SO<sub>4</sub><sup>2-</sup>, control REE mobility (Hass *et al.*, 1995).

However, based on tetrad patterns involving the distribution coefficient, Veksler *et al.* (2006) concluded that only silicate melts produce M-shaped patterns. The conjugate fluoride liquid, on the other hand, should be W-shaped. Masuda *et al.* (1987) distinguished two types of tetrad effects: M-type and W-type (M-type in solid sample as residues and W-type in the interacting fluids as extract). The tetrad effect values were calculated using Irber's (1999) quantification method:

$$t_1 = (Ce/Ce^* \times Pr/Pr^*), t_3 = (Tb/Tb^* \times Dy/Dy^*), t_4 = (Tm/Tm^* \times Yb/Yb^*)$$

$$\text{Degree of the tetrad effect } TE_{1,3} = (t_1 \times t_3)^{0.5}$$

The REE tetrad effect was mainly observed in late magmatic differentiation related to strong hydrothermal interactions or deuteric alteration (Jahn *et al.*, 2001).

The calculated values of the tetrad effect have an average of 1.14. For a REE pattern without tetrad effect are samples with values of  $TE_{1,3} < 1.1$ , where at  $TE_{1,3} > 1.1$  the tetrad effect become well visible. The M-shaped pattern shows  $TE_i > 1.1$  and the W-shaped -  $TE_i < 0.9$ . The use of first, third and fourth tetrads ( $TE_{1,4}$ ) gives a rather correct estimation.

The Chondrite-normalized REE patterns of the lamprophyre show M-type tetrad effect is similar to that quoted by Masuda *et al.* (1987) in most samples, with the exception of sample No. 1, which has  $t_4$  W-type tetrad (Fig.11), suggesting the presence of convex-concave tetrad, confirming the effect of water-rich phase in lamprophyre samples. M-W type tetrad effect may be related to the interaction of aqueous liquids with alkaline rocks (Zhao *et al.*, 2008; Cao *et al.*, 2013; El Mezayen *et al.*, 2015, 2019). The changes in the physico-chemical conditions could be connected to the presence of M-W type tetrad in the lamprophyre samples (Mahdy and El-Kammar, 2003). The peculiar M-W type tetrad effect could be an indication of Au mineralization (Zhao *et al.*, 2010; El Mezayen *et al.*, 2020; Sallam *et al.*, 2021) which confirmed by the presence of gold grains in the heavy fractions of the studied samples.

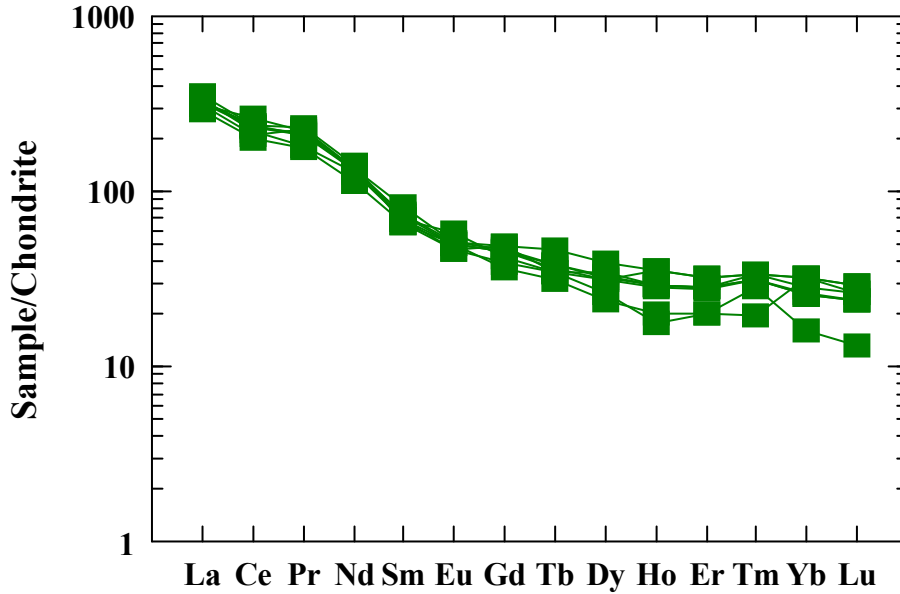


Fig. 11. Chondrite normalized (Sun and McDonough, 1989), REE pattern for the lamprophyre samples

4.3.2. Post-magmatic alteration and crustal contamination

4.3.2.1. Alteration index

This index was defined by Ishikawa *et al.* (1976) to quantify the intensity of sericite and chlorite alteration in magmatic rocks. Ishikawa alteration index (AI) with chlorite-carbonate-pyrite index (CCPI). The AI reflects the ratio of the principal rock-forming elements that were gained ( $K_2O + MgO$ ) during chlorite and sericite alteration with the total elements that were gained and lost ( $K_2O + MgO + Na_2O + CaO$ ).

$AI = 100 * (K_2O + MgO) / (K_2O + MgO + Na_2O + CaO)$ . The CCPI is based on major elements and was defined as:  $CCPI = 100 * (MgO + FeO) / (MgO + FeO + Na_2O + K_2O)$ . The Ishikawa (AI) index was defined by Foley *et al.* (1987) to quantify the intensity of sericite and chlorite alterations. The alteration box plot is a useful way for discriminating geochemical trends due to diagenetic alteration from those due to hydrothermal alteration directly related to sulfide ores.

In general, all of the lamprophyre samples exhibit low to intermediate degree of alterations and plot in the hydrothermal alteration field (Fig. 12). The lamprophyre samples plot close to trend no. 4 (chlorite-carbonate), alterations typically developed immediately adjacent to massive sulfide lenses (Taylor and McLennan, 1980).

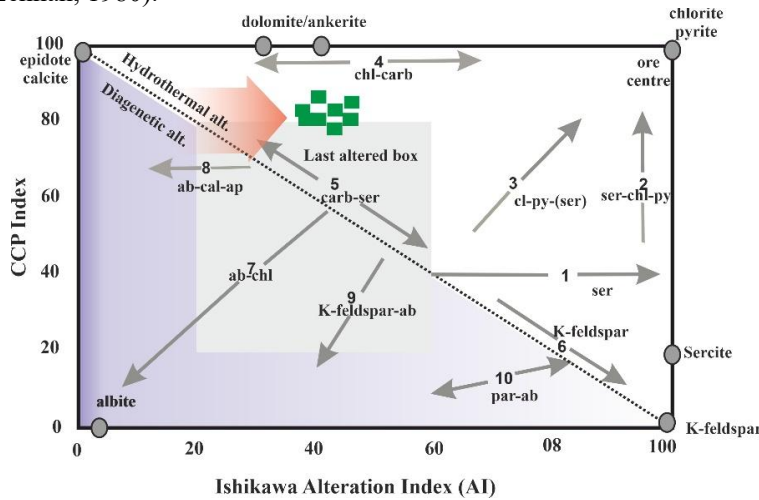
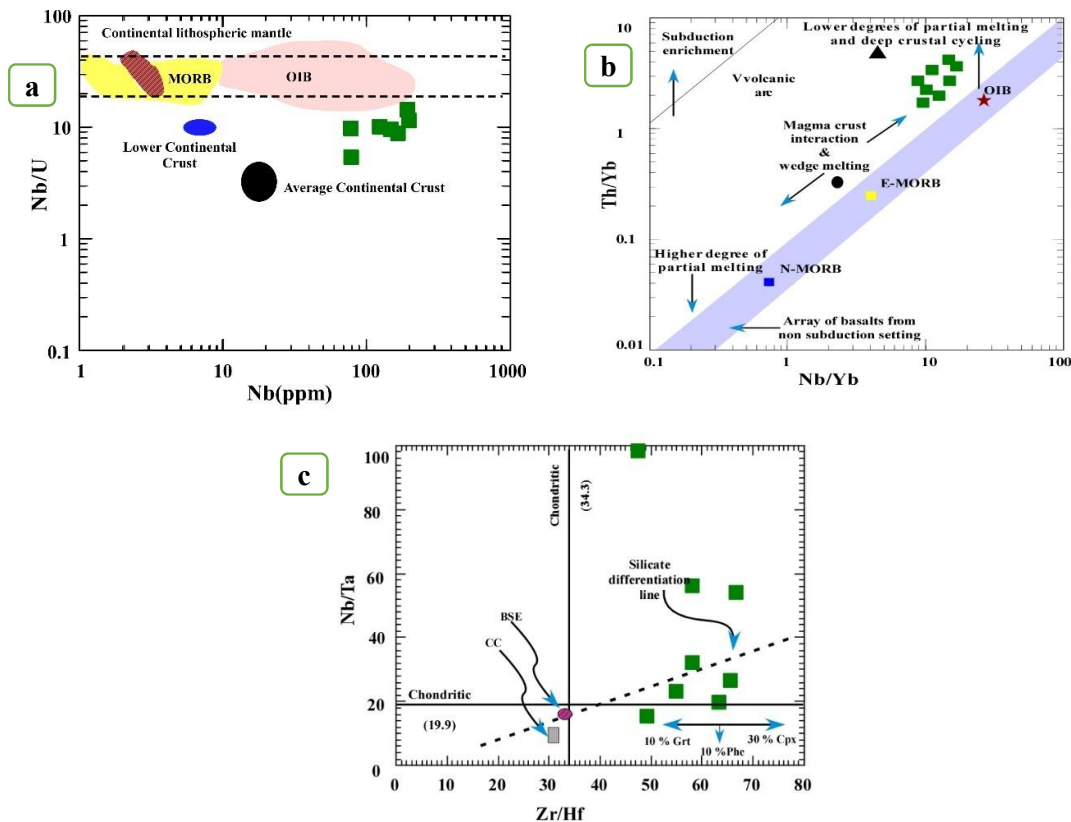


Fig. 12: Hydrothermal and diagenetic alteration box plot diagrams (after Large *et al.*, 2001)

#### 4.3.2.2. Crustal contamination and Petrogenesis of the lamprophyre dyke

Crustal contamination and alteration (dueteric) of minerals in lamprophyres during emplacement is a common process (Rock, 1991; Moyer *et al.*, 2003). Therefore, it is necessary to assess the effect of crustal contamination and alteration before the interpretation of geochemical data. Crustal rocks are known to be enriched in LILEs, and have negative Nb and Ta anomalies, whereas their major oxides show high content of K<sub>2</sub>O and Na<sub>2</sub>O with depleted TiO<sub>2</sub> and P<sub>2</sub>O<sub>5</sub> contents. However, high concentrations of REE and incompatible trace elements, and lower degrees of partial melting, make lamprophyres insensitive to crustal contamination.

The continental crust is characterized by Lu/Yb ratios (0.16–0.18) (Sun and McDonough, 1989). Th/La values range from 0.02 to 0.23, with values of < 0.12 indicating insignificant crustal contamination; while values of > 0.12 imply evident crustal contamination. Our studied samples have Lu/Yb (Av.0.15) and Th/La (Av.0.13) ratios indicating minor crustal contamination. Higher Nb/U (Av. 9.5) and Ce/Pb (Av. 1.2) of the lamprophyre samples also are different from those of crustal values (Nb/U = 6.15; Ce/Pb = 3.91, Rudnick and Gao, 2003). The Nb versus Nb/U diagram (Fig. 13 a) demonstrate the similarity of the lamprophyre samples plots, where they lie close to the field of the average continental crust.



**Fig. 13:** a) Nb (ppm) vs Nb/U (Ma *et al.*, 2013). b) Nb/Yb vs Th/Yb diagram (after Menzies and Kyle, 1990). c) Zr/Hf vs. Nb/Ta diagram for the studied lamprophyre. Data for Tanzanian peridotites from Rudnick *et al.*, 1993; for mid-oceanic ridge basalt (MORB) from Sun and McDonough and for oceanic island basalts (OIB) from Foley *et al.*, 2002. The silicate differentiation line in the diagram is taken from Münker *et al.*, 2003 and indicates first order coupling of Nb/Ta–Zr/Hf due to fractionation of the silicate mantle by melting processes. The average composition of the continental crust (CC) is taken from Barth *et al.* (2000). Vector for garnet (Grt) is given to illustrate fractionation during melt–peridotite interaction with partition coefficients from Rubatto & Hermann (2007); 1000°C run). Vector for phengite (Phe) is given to illustrate the effect of buffering mica on Nb/Ta during partial melting of subducted continental crust (Stepanov & Hermann, 2013; 1000°C run).

Trace element ratios like Th/Yb, Ta/Yb, Nb/U, and Ce/Pb are widely known to be unaffected by magmatic processes and reflect their source regions. As a result, these ratios are used as petrogenetic markers (c.f. Hofmann, 1997). The Th/Yb vs Nb/Yb diagram has also been discovered to be beneficial in determining crustal contamination. (Fig. 13b).

During crustal contamination processes, Th is more affected than Ta and Yb (Gourgaud and Vincent, 2004). As a result, rocks with crustal contamination have high Th/Yb values and act along the active continental margin (Wilson, 1989).

The Zr/Hf and Nb/Ta fractionation displayed by the samples (Fig. 13c) strongly suggests the role of rutile-rich metasomatic imprints on their source regions. These ratios are higher than those of the average crust and mantle, suggests the presence of residual Hf, Ta-bearing titanates in their source (cf. Lavecchia *et al.*, 2006; Tappe *et al.*, 2008). Thus, the effect of crustal contamination on magma evolution of the lamprophyres may be limited.

HREE fractionation in mafic lavas is typically caused by the melting of a garnet-containing mantle source or by mantle enrichment with fluids/melts released from garnet-bearing subducted sediments (Avanzinelli *et al.*, 2008; O'Neill, 1981).

Assuming non-modal batch melting of a garnet-bearing PM (Sun and McDonough, 1989) and EAM (enriched asthenospheric mantle), (Seghedi *et al.*, 2004) as source compositions, we determined the extent of partial melting (Fig. 14a) (see Miller *et al.*, 1999). According to these calculations, lamprophyre magmas could occur from EAM melting at a rate of 2 to 10%, followed by fractionation (Fig.14b). According to Kostopoulos and James (1992), the suggested EAM might have contained garnet (curve A) or spinel (curve B) using non-modal batch melting equations and a melting model of an enhanced asthenospheric mantle source (EAM), (Seghedi *et al.*, 2004).

Melting curves for garnet lherzolite (Kostopoulos and James, 1992, curve C), garnet-amphibole lherzolite (Barry *et al.*, 2003, curve D), and another garnet amphibole lherzolite with slightly different composition than the latter (new calculations, curve E) have been calculated using EAM as the source material (Fig.14b). According to the estimates, partial melting of an enhanced garnet peridotite mantle source occurs at 2–10%. Lamprophyre samples, on the other hand, have an average primitive mantle-normalized Sm/Yb ratio of 2.4, which is compatible with melting in the presence of residual garnet (McKenzie and O'Nions, 1991; Orejana *et al.*, 2008). According to the latter, the spinel-garnet transition zone is 75–85 kilometers deep.

The sampled lamprophyres were plotted in the  $K/Yb*1000 - Dy/Yb$  plot to determine the nature of the protolith, mantle source, and degree of partial melting (Duggen *et al.*, 2005; Jiang *et al.*, 2010) (Fig.14 c). This plot distinguishes partial melting in the spinel garnet stability fields of a phlogopite and/or amphibole bearing lherzolite/peridotite and is used to limit the composition of the mantle source and the degree of partial melting. The Dy/Yb ratio of the lamprophyres sampled ranges from 1.1 to 2. The partial melting of 2 to 10% is indicated by the data points placed along the garnet amphibole lherzolite curve. As a result, it's possible that the lamprophyres are generated in the spinel-garnet transition zone at 75–85 km deep by low-degree partial melting of phlogopite/amphibole-bearing lherzolite ranging from 2 to 10%.

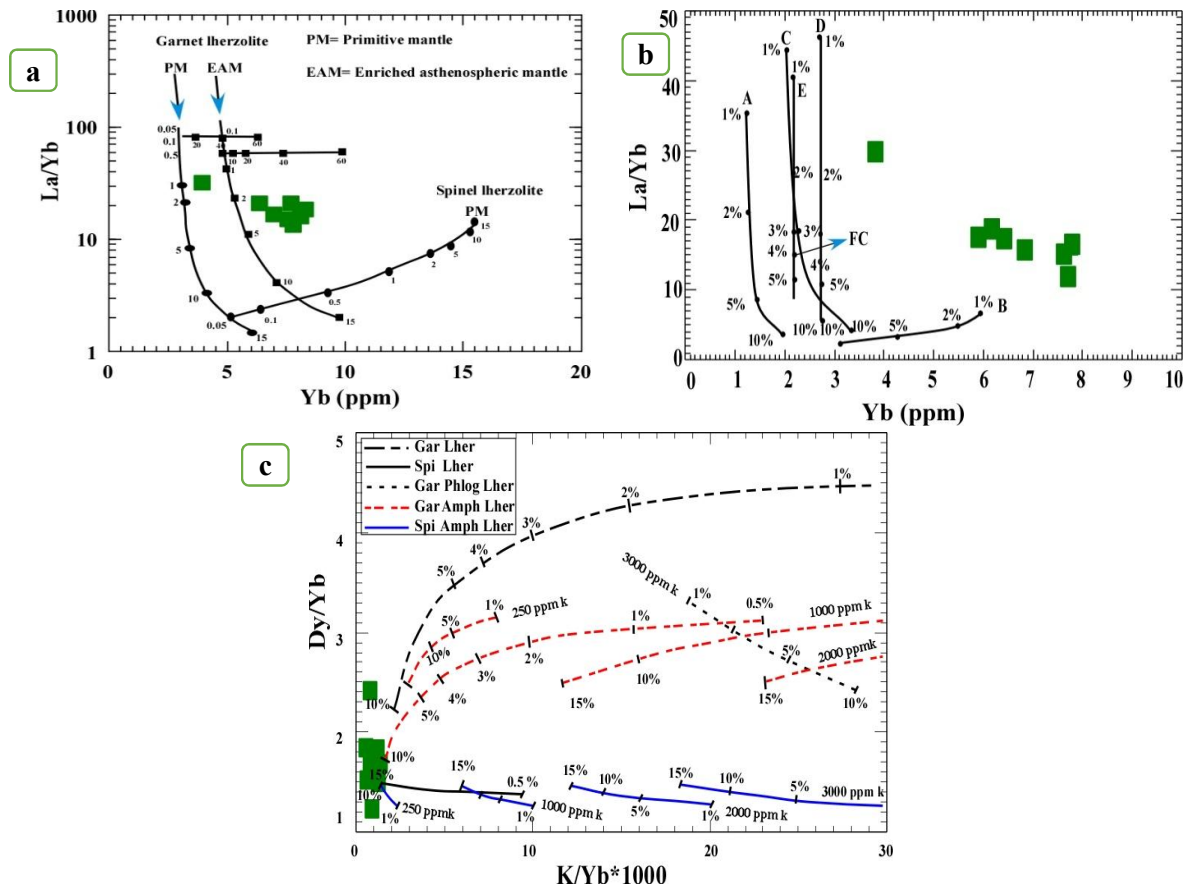


**Fig. 14.** (a), (b) La/Yb vs. Yb (ppm) plot for lamprophyre samples with melting curves assuming non-modal batch melting of garnet bearing PM (primitive mantle) and EAM (enriched asthenospheric mantle) as source. Initial modal mineralogy: Ol (55%) + Opx (19%) + Cpx (7%) + Gnt (11%) + Phl (8%) and melting phase proportions: Ol (5%) + Opx (12%) + Cpx (20%) + Gnt (40%) + Phl (23%) have been taken from Miller *et al.* (1999). Partition coefficients for olivine, pyroxene and garnet have been taken from Kostopoulos and James (1992), whereas those for phlogopite are from Fujimaki *et al.* (1984). Array for the fractional crystallization (FC) assuming fractionation of olivine (40%) and clinopyroxene (60%) has also been shown for every 10% increment. Degree of partial melting has been shown along the tick marks. C) K/Yb\*1000 – Dy/Yb (after Duggen *et al.*, 2005; Jiang *et al.*, 2010). Melting curves for garnet lherzolite, spinel lherzolite, garnet-facies phlogopite lherzolite, garnet-facies amphibole lherzolite and spinel-facies amphibole lherzolite are after Duggen *et al.* (2005).

## 5. Conclusions

The tectono-stratigraphic sequence begins from the oldest to youngest as follows; psammitic gneisses, ophiolitic mélangé, monzogranite, and lamprophyre dykes. Microscopic investigation of the lamprophyres of W. Sikait area indicates that they are mostly spessartites and kersantite. The ESEM/EDX of heavy minerals revealed the dominance of large mineral assemblages that include monazite-allanite, yttracolumbite, gold, cassiterite, wolframite, galena, and native nickel.

The lamprophyre dykes are basalt to basanite/tephrite in composition, ultrabasic, highly potassic, and calc-alkaline in character. Lamprophyres are also known to be spatially and temporally associated with gold mineralization, for example, orogenic gold deposits. Rock (1991) considered lamprophyres as a possible source rock for gold (Müller and Groves, 2019), but this view is not generally supported. The more reasonable explanation for the correlation is that lamprophyres, representing "wet" melt of the asthenosphere and mantle, correlate with a period of high fluid flow from the mantle through the crust, during subduction-related metamorphism, which drives gold mineralization.

The lamprophyres are suggested to be derived from a mantle source spatially related to a shallow to moderately deep subduction tectonic setting within the spinel – garnet transition depths. Low to

moderate degrees of partial melting of the source generated the parental melts which were emplaced near the mantle wedge region where the subducting plate contributed slab related materials to the mantle wedge region. Interaction of the parental melts and slab materials occurred at the mantle wedge producing the lamprophyric melts. This process probably added LILE and selected HFSE to the generated lamprophyric melts. These melts appear to have been emplaced later in a staggered manner into and along fracture systems related to pre-existing crustal lineaments in their host rocks to generate the lamprophyre dykes by fractional crystallization and differentiation.

### Acknowledgment

The authors sincerely thank the late prof. Mohamed E. Ibrahim for suggesting the research point. Also, thanks to Professors Gehad M. Saleh and Mohamed G. El Feky for their revisions and critical comments.

### References

- Avanzinelli, R., T. Elliot, S. Tommasini and S. Conticelli, 2008. Constraints on the genesis of potassium-rich Italian volcanic rocks from U/Th disequilibrium. *J Petrol* 49:195–223.
- Barry, T. L., A. D. Saunders, P. D. Kempton, B. F. Windley, M. S. Pringle, D. Dorjnamjaa and S. Saandar, 2003. Petrogenesis of Cenozoic basalts from Mongolia: evidence for the role of asthenospheric versus metasomatized lithospheric mantle sources. *J. Petrol.* 44 55–91.
- Barth, M.G., W.F. McDonough and R.L. Rudnick, 2000. Tracking the budget of Nb and Ta in the continental crust. *Chemical Geology* 165: 197–213.
- Berger, A., E. Gnos, E. Janots, A. Fernandez and J. Giese, 2008. Formation and composition of rhabdophane, bastnasite and hydrated thorium minerals during alteration: Implications for geochronology and low-temperature processes. *Chemical geology*, 254 (3-4) :238-248.
- Bergman, S. C., 1987. Lamproites and other K-rich igneous rocks: review of their occurrence, mineralogy and geochemistry. In: *Alkaline Igneous Rocks*, J. G. Fulton and B. J. G. Upton (eds.), Spl. Publ. Geol. Soc. London, 30, 163-190.
- Cao, M.J., G.M. Li, K.Z. Qin, E.Y. Seitmuratova and Y.S. Liu, 2013. Major and trace element characteristics of apatites in granitoids from Central Kazakhstan: implications for petrogenesis and mineralization. *Resour Geol.*, 62:63–83.
- Cox, K.G., J.D. Bell and R.J. Pankhurst (1979): *The interpretation of igneous rocks*. George Allen and Unwin, London.
- Cullers, R.L. and J. Graf, 1984. Rare Earth Element in Igneous Rocks of the Continental Crust: Intermediate and Silicic Rocks, Ore Petrogenesis. In: Henderson, P., Ed., *Rare Earth Geochemistry*, Elsevier, Amsterdam, 275-316.
- Currie, K.L. and P.R. Williams, 1993. An Archean calc-alkaline lamprophyre suite, northeastern Yilgarn Block, western Australia. *Lithos*, 31, 33–50.
- Da Silva, Gabriel, 2004. "Kinetics and mechanism of the bacterial and ferric sulphate oxidation of galena". *Hydrometallurgy*, 75: 99. doi:10.1016/j.hydromet.2004.07.001
- Duggen, S., K. Hoernle, P.V.D. Bogaard and D. Garbeschönberg, 2005. Post collisional Transition from subduction to Intraplate type magmatism in the western most Mediterranean: evidence for continental edge delamination of subcontinental lithosphere. *Journ. Petro.* v46. Pp 1155 to 1201.
- El Bayoumi RM (1980): *Ophiolites and associated rocks of Wadi Ghadir, east of Gabal Zabara, Eastern Desert, Egypt*. Unpublished Ph.D. Thesis, Univ. Cairo, 227 pp.
- El Mezayen, A. M., M. G. El-Feky, A.O. Sayed and I. Sherif Abd El Aziz, 2015. Geochemistry and a composite M- with W-type of REE tetrad effect in altered granites of Abu Furad area, Central Eastern Desert, Egypt. *Greener Journal of Geology and Earth Sciences*, 3(2):013-029. <http://doi.org/10.15580/GJGES.2015.2.111915161>.
- El Mezayen, A. M., M. A. Heikal, M. G. El-Feky, H. A. Shahin, I. K. Abu Zeid and S. R. Lasheen 2019. Petrology, geochemistry, radioactivity, and M–W type rare earth element tetrads of El Sela altered granites, South Eastern Desert, Egypt. *Acta Geochim* 38(1):95–119. <https://doi.org/10.1007/s11631-018-0274-7>.
- El Mezayen, A. M., E.K. Abu Zeid, M.G. El-Feky, A.O. Sayed, H.A. Ali, S.A. Taala, 2020. Mineralogical and Geochemical studies on Kab Amiri Altered Granitic Rocks and Associated Pegmatite, Central Eastern Desert, Egypt. *IJMS*, 6, 2, 11-33.

- El Tohamy, A. M., 2019. Mineralogy and geochemistry of the Sikait U-Au-bearing lamprophyre dyke, South Eastern Desert, Egypt. *Arab. J. of Geo.*, 12, 237.  
<https://doi.org/10.1007/s12517-019-4394-0>
- El-Balakssy, S. S., W. H. Saleh and M. O. EL-Husseiny, 2012. Characterization of accessory allanite from Um Lassifa granites, Central Eastern Desert, Egypt. *Al-Azhar Bull. Sci.* Vol. 23, No. 1 (June.): 1-28.
- Foley, S.F., A.V. Andronikov and S. Melzer, 2002. Petrology, geochemistry and mineral chemistry of ultramafic lamprophyres from the Jetty Peninsula area of the Lambert-Amery Rift, Eastern Antarctica. *Mineral Petrol.*, 74:361–384.
- Foley, S.F., G. Venturelli, D.H. Green and L. Toscani, 1987. The ultrapotassic rocks: characteristics, classification and constraints for petrogenetic models. *Earth-Sci Rev.*, 24:81–134.
- Foley, S. F., 1992. Vein-plus-wall-rock melting mechanisms in the lithosphere and the origin of potassic alkaline magmas, *Lithos*, 28, 435–453. doi:10.1016/0024-4937(92)90018-T.
- Fowler, A.R. and A.F. Osman, 2009. The Sha'it-Nugrus shear zone separating Central and South Eastern Deserts, Egypt: a post-arc collision low-angle normal ductile shear zone. *J Afr Earth Sci.*, 53,16–32.
- Fowler, M.B. and P.J. Henney, 1996. Mixed Caledonian appinite magmas: implications for lamprophyre fraction and high Ba-Sr granite genesis. *Contributions to Mineralogy and Petrology* 126,199–215.
- Fritz, H., E. Wallbrecher, A.A. Khudier, F. Abu El Ela and R.D. Dallmeyer, 1996. Formation of Neoproterozoic metamorphic core complexes during oblique convergence, Eastern Desert, Egypt. *J Afr Earth Sci.*, 23,311–329.
- Fron del, C., 1958. Systematic mineralogy of uranium and thorium, US Geological Survey Bulletin, 1064, US Government Printing Office, Washington, 400p.
- Fujimaki, H., M. Tatsumoto and K. I. Aoki, 1984. Partition coefficients of Hf, Zr, and REE between phenocrysts and groundmasses; *J. Geophys. Res.*, (Solid Earth) 89 662– 672.
- Furman, T., and D. Graham, 1999. Erosion of lithospheric mantle beneath the East African Rift system: evidence from the Kivu volcanic province. *Lithos*. 48, 237 - 262.
- Gourgaud, A., P.M. Vincent, 2004. Petrology of two continental alkaline intraplate series at Emi Koussi volcano, Tibesti, Chad. *J Volcanol Geotherm Res.*, 129:261–290.
- Greiling, R.O., A. Kröner, M.F. El Ramly and A.A. Rashwan, 1988. Structural relationships between the southern and central parts of the Eastern Desert of Egypt: details of a fold and thrust belt. In: El Gaby, S., Greiling, R.O. (Eds.). *The Pan-African Belt of Northeast Africa and Adjacent Areas*. Vieweg and Sohn, Weisbaden, 121– 145.
- Hass, J.R., E.L. Shock, and D.C. Sassani, 1995. Rare earth elements in hydrothermal system: Estimates of standard partial model thermodynamic properties of aqueous complexes of the rare earth elements at high pressure and temperature. *Geochim. Comochim Acta*, v. 59, p. 4329-4335.
- Hofmann, A.W., 1997. Mantle geochemistry: the message from oceanic 10volcanism. *Nature* 385:219–229.
- Huang, Z., C. Liu, H. Yang, C. Xu, R. Han, Y. Xiao, B. Zhang and W. Li, 2002. The geochemistry of lamprophyres in the Laowangzhai gold deposits, Yunnan Province, China: implications for its characteristics of source region. *Geochemical Journal*, 36, 91–112.
- Ibrahim, I.H., 2013. Abu Rusheid-Sikait Mylonitic Rocks, South Eastern Desert, Egypt: Origin and Mode of Occurrence. *International Conference on Natural Hazards and Geomatics -ICNHG*, Tunisia.
- Ibrahim, M. E., K. Watanabe, G. M. Saleh, W. S. Ibrahim, 2015. Abu Rusheid lamprophyre dikes, South Eastern Desert, Egypt: as physical-chemical traps for REEs, Zn, Y, U, Cu, W, and Ag. *Arab J Geosci*. DOI 10.1007/s12517-015-1882-8.
- Ibrahim, M.E. and A.A. Ragab, 2011. Geochemistry of lamprophyre dykes, Wadi Sikait area, South Eastern Desert, Egypt. *Chin. J. Geochem.*, 30, 323–331.  
<https://doi.org/10.1007/s11631-011-0516-4>.
- Ibrahim, M.E., B.A. El- Kalioby, G.M. Aly, A.M. El-Tohamy and W. Koichiro, 2015. Altered granitic rocks, Nusab El Balgum Area, Southwestern Desert, Egypt: Mineralogical and Geochemical Aspects of REEs. *Ore Geology Reviews*, 70, 252-261.  
<https://doi.org/10.1016/j.oregeorev.2015.04.016>.

- Irber, W., 1999. The lanthanide tetrad effect and its correlation with K/Rb, Eu/Eu\*, Sr/Eu, Y/Ho, and Zr/Hf of evolving peraluminous granite suites. *Geochimica et Cosmochimica Acta* 63, 489–508.
- Ishikawa, Y., T. Sawaguchi, S. Iwaya, M. Horiuchi, 1976. Delineation of prospecting targets for Kuroko deposits based on modes of volcanism of underlying dacite and alteration halos. *Mining Geol.* 26, 105–117.
- Jahn, B. M., F. Wu, R. Capdevila, F. Martineau, Z. Zhao and Y. Wang, 2001. Highly evolved juvenile granites with tetrad REE patterns: the Woduhe and Baerzhe granites from the Great Xing'an Mountains in NE China. *Lithos*, 59, 171–198.
- Jiang, Y. H., S. Y. Jiang, H. F. Ling and P. Ni, 2010. Petrogenesis and tectonic implications of Late Jurassic shoshonitic lamprophyre dikes from the Liaodong Peninsula, NE China; *Min. Petrol.* 100 127–151.
- Kamar, M.S., 2021. Geochemical and Mineralogical Studies of the Mylonite Xenoliths and Monzogranite Rocks at Wadi Abu Rusheid, South Eastern Desert, Egypt: Insights on the Genesis of Mineralization. *Acta Geologica Sinica (English Edition)*, 95(5): 1551–1567.
- Kamar, M. S., A. M. El Tohamy, H. I. Mira and A.M. Ismail, 2022. Geology and Environmental Impact Assessment of Psammitic Gneiss and Lamprophyre Dykes at Wadi Sikait, South Eastern Desert, Egypt. 11st International Conference on chemical and environmental engineering ICEE.
- Kepezhinskas, P., F. McDermott, M.J. Defant, A. Hochstaedter, M.S. Drummond, C.J. Hawkesworth, A. Koloskov, R. C. Maury and H. Bellon, 1997. Trace element and Sr-Nd-Pb isotopic constraints on a three-component model of Kamchatka Arc petrogenesis: *Geochimica et Cosmochimica Acta*, 61, 577–600.  
doi:10.1016/S0016- 7037(96)00349-3.
- Kepezhinskas, P.K., G.M.D. Eriksen, N.P. Kepezhinskas, 2016. Geochemistry of Ultramafic to Mafic Rocks in the Norwegian Lapland: Inferences on Mantle Sources and Implications for Diamond Exploration, *Earth Science Research*, 5, 148-187.
- Kostopoulos, D.K. and S.D. James, 1992. Parametrization of the melting regime of the shallow upper mantle and the effects of variable lithospheric stretching on mantle modal stratification and trace element concentrations in magmas. *Journal of Petrology*, 33, 665– 691.
- Large, R., J.B. Gemmill, H. Paulick and D.L. Huston, 2001. The Alteration Box Plot: A simple approach to understanding the relationship between alteration mineralogy and litho-geochemistry associated with Volcanic-Hosted Massive Sulfide deposits. *Econ. Geol.* 96, 957–971.
- Lavecchia, G., F. Stoppa and N. Creati, 2006. Carbonatites and kamafugites in Italy: mantle-derived rocks that challenge subduction. *Ann Geophys*, 49(1):389–402.
- Le Maitre, R.W., 1989. A Classification of Igneous Rocks and Glossary of Terms: Recommendations of the International Union of Geological Sciences, Subcommission on the Systematics of Igneous Rocks. Blackwell, Oxford. 193 pp.
- Le Roex, A.P., D.R. Bell, and P. Davis, 2003. Petrogenesis of group I kimberlites from Kimberley, South Africa: evidence from bulk-rock geochemistry. *Journal of Petrology*, 44, 2261–2286.
- Lefebvre, N., M. Kopylova and K. Kivi, 2005. Archean calc-alkaline lamprophyres of Wawa, Ontario, Canada: Unconventional diamondiferous volcanoclastic rocks. *Precambrian Research*, 138, 57–87.
- Ma, L., S.Y. Jiang, L. Hou, B.Z. Dai, Y.H. Jiang, T. Yang, K.D. Zhao, W. Pu, Z.Y. Zhu, B. Xu, 2013. Geochemistry of early cretaceous calc-alkaline lamprophyres in the Jiaodong peninsula: implication for lithospheric evolution of the eastern North China craton. *Gondwana Res.*, 25: 859–872.
- Madhavan, V., K. David, J. Mallikharjuna Rao, N.V. Chalapathi Rao and M. Srinivas, 1998. Comparative study of lamprophyres from the Cuddapah Intrusive Province (CIP) of Andhra Pradesh, India. *Journal of Geological Society of India*, 52, 621-642.
- Mahdy A.I. and A.M. El-Kammar, 2003. Geochemical Partitioning of Isovalent and Tetrad Effect of REE Associating Episynitization of Kab Amiri Granites, Central Eastern Desert of Egypt C. pp.111–125. 5<sup>th</sup> In. Conf. of Geology of Middle East Cairo Egypt.
- Masuda, A., O. Kawakami, Y. Dohmoto and T. Takenaka, 1987. Lanthanide tetrad effects in nature: two mutually opposite types, W and M. *Geochemical Journal* 21, 119–124.
- McDonough, W. F. and S. S. Sun, 1995. The composition of the Earth. *Chem. Geol.* 120, 223–253.

- McKenzie, D. and R. K. O’Nions, 1991. Partial melt distributions from inversion of rare earth element concentrations; *J. Petrol.*, 32 1021–1091.
- McKenzie, D.P., 1989. Some remarks on the movement of small melt fractions in the mantle. *Earth and Planetary Science Letters*, 95, 53–72.
- McLennan, S.M., B.J. Fryer and G.M. Yound, 1979. Rare earth elements in Huronian (lower Proterozoic) sedimentary rocks: composition and evolution of the postkenoran upper crust. *Geochim Cosmchim Acta*, 43:375–388.
- Menzies, M.A. and P. Kyle, 1990. *The continental mantle*. Clarendon Press, Oxford, pp 157–177.
- Miller, C., R. Schuster, U. Klötzli, W. Frank and F. Purtscheller, 1999. Post–collisional potassic and ultrapotassic magmatism in SW Tibet: Geochemical and Sr–Nd–Pb–O isotopic constraints for mantle source characteristics and petrogenesis *Journal of Petrology*, 40, 1399–1424.
- Morin, J. A., 1977. Allanite in granitic rocks of the Kenora –Vermilion Bay area, northwestern Ontario. *Can. Mineral.*, 15, 297-302.
- Moyen, J.F., H. Martin, M. Jayananda and B. Auvray, 2003. Late Archaean granites: a typology based on the Dharwar craton (India). *Precambrian Research*, 127, 102–123.
- Muller, D. and D.I. Groves, 2019. Tectonic settings of Potassic Igneous rocks In *Potassic Igneous Rocks and Associated Gold–Copper Mineralization*. *Mineral Resource Reviews*, 31–71.
- Münker, C., J.A. Pfänder, S.Weyer, A. Büchl, T. Kleine and K. Mezger, 2003. Evolution of planetary cores and the Earth–Moon system from Nb/Ta systematics. *Science* 301: 84–87.
- O’Neill, H.S., 1981. The transition between spinel lherzolite and garnet lherzolite, and its use as a Geobarometer. *Contrib Mineral Petrol* 77:185–194
- Orejana, D., C. Villaseca, K. Billström and B. A. Paterson, 2008. Petrogenesis of Permian alkaline lamprophyres and diabases from the Spanish Central System and their geodynamic context within western Europe; *Contrib. Mineral. Petrol.*, 156 477–500.
- Pearce, J.A., 1983. The role of sub-continental lithosphere in magma genesis at destructive plate margins. In: Hawkesworth, C.J., Norry, M.J. (Eds.), *Continental Basalts and Mantle Xenoliths*. Shiva, Nantwich, pp. 230–249.
- Prelevic, D., S.F. Foley, V. Cvetkovi and R.L. Romer, 2004. Origin of Minette by Mixing of Lamproite and Dacite Magmas in Veliki Majdan, Serbia. *Journal of Petrology* 45, 759–792.
- Rock, N.M., 1987. The nature and origin of lamprophyres: an overview. In: Fitton JG, Upton BGJ (eds) *Alkaline Igneous Rocks*. Geological Society Special Publications, 30. Geological Society of London, London, pp 191–226
- Rock, N.M., 1991. Lamprophyres. In: Rock NMS, Groves DI (eds) 1988. *Can lamprophyres resolve the genetic controversy over mesothermal gold deposits*. *Geology*, vol 16. Blackie, Glasgow, pp 1–285, 538–541.
- Rubatto, D. and J. Hermann, 2007. Experimental zircon/melt and zircon/garnet trace element partitioning and implications for the geochronology of crustal rocks. *Chemical Geology*, 241: 38–61.
- Rudnick, R.L. and S. Gao, 2003. Composition of the continental crust. In *The Crust* (Holland, H.D. and Turekian, K.K. Eds.). *Treatise on Geochemistry*, 3, 1–64. Rogers NW, Hawkesworth CJ, Mathey DP, Harmon RS (1987) *Sediment subduction and the source of potassium in orogenic leucitites*. *Geology*, 15:451-453.
- Ryan, J., J. Morris, G. Bebout and B. Leeman, 1996. Describing chemical fluxes in subduction zones: insights from “depth profiling” studies of arc and forearc rocks, In: Bebout, G.E., Scholl, D.W., Kirby, S.H., Platt, J.P., (Eds.), *Subduction Top to Bottom*, American Geophysical Union, Washington DC, pp. 263-268.
- Saleh, G.M., 1997. The potentiality of uranium occurrences in Wadi Nugrus area, South Eastern Desert, Egypt. Ph. D. Thesis mans. Univ., p 171
- Saleh, G.M., S.A. Abdallah, A.A. Abbas, N.A. Dawood and M.A. Rashed, 2012. Uranium mineralizations of Wadi Sikait mylonites, Southeastern Desert, Egypt. *J. of Geo. and Min. Res.* 3(5), 86-104. <https://doi.org/10.5897/JGMR10.035>
- Sallam, O. R., H. I. Mira, A. M. El-Tohamy, and A. A. Abbas, 2021. Mineralogy and Geochemistry of Uraniferous Sandstones in Fault Zone, Wadi El Sahu Area, Southwestern Sinai, Egypt: Implications for Provenance, Weathering and Tectonic Setting. *Acta Geologica Sinica (English Edition)*, 95(3): 830–845. <https://doi.org/10.1111/17556724.14613>.

- Seghedi, I., H. Downes, O. Vaselli, A. Szaka'cs, et al. 2004. Postcollisional Tertiary–Quaternary mafic alkalic magmatism in the Carpathian–Pannonian region: a review. *Tectonophysics*, 393, 43–62.
- Stepanov, A.S. and J. Hermann, 2013. Fractionation of Nb and Ta by biotite and phengite: Implications for the “missing Nb paradox”. *Geology*, 41: 303–306.
- Sun, S.S. and W.F. McDonough, 1989. Chemical and isotopic systematics of ocean basalts: implications for mantle composition and processes. *Geol Soc Spec Publ.*, 42:313–345.
- Tappe, S., S.F. Foley, G. A. Jenner, L. M. Heaman, B. A. Kjarsgaard, R. L. Romer, A. Stracke, N. Joyce and J. Hoefs, 2006. Genesis of ultramafic lamprophyres and carbonatites at Aillik Bay, Labrador: a consequence of incipient lithospheric thinning beneath the North Atlantic craton; *J. Petrol.* 47 1261–1315.
- Tappe, S., S.F. Foley, B.A. Kjarsgaard, R.L. Romer, L.M. Heaman, A. Stracke and G.A. Jenner, 2008. Between carbonatite and lamproite. Diamondiferous Torngat ultramafic lamprophyres formed by carbonate-fluxed melting of cratonic MARID-type metasomes. *Geochim Cosmochim Acta*, 72:3258–3286.
- Taylor, S.R., R. Arculus, T.R. Perfi and R.W. Johnson, 1981. Island arc basalts. In: Merrill RB, Ridings R (eds) *Basaltic volcanism on the terrestrial planets*. Pergamon, New York, pp 193–213.
- Taylor, S.R. and S.M. McLennan, 1980. The rare earth elements evidence in Precambrian sedimentary rocks: implication for crustal evolution. In: Kroner A (ed) *Precambrian plate tectonic*. Elsevier, Amsterdam.
- Thompson, R.N., P.T. Leat, A.P. Dickin, M.A. Morrison, G.L. Hendry and S.A. Gibson, 1990. Strongly potassic mafic magmas from lithospheric mantle source during continental extension and heating: evidences from Miocene minettes of northwest Colorado, U.S.A. *Earth and Planetary Science Letters*, 98, 139–154.
- Veksler, I., A. Dorfman, L. Danyushevsky, J. Jakobsen and D. Dingwell, 2006. Immiscible silicate liquid partition coefficients: implications for crystal-melt element partitioning and basalt petrogenesis. *Contributions to Mineralogy and Petrology* 152: 685-702.
- Wilson, M., 1989. *Igneous petrogenesis: a global tectonic approach*. Unwin Hyman, Boston 466pp.
- Young, Courtney A., Taylor Patrick R., Anderson Corby G., 2008. *Hydrometallurgy 2008: Proceedings of the Sixth International Symposium*. SME. ISBN 9780873352666.
- Zhang, Y., B. Chen, J.A. Shao and M.G. Zhai, 2003. Geochemistry and origin of late Mesozoic lamprophyre dykes in Aihang mountains, north China. *Acta Petrologica ET Mineralogica* 22, 29–33 (in Chinese with English abstract).
- Zhao, Z. H., Z. W. Bao, Lee Seung-Gu, et al., 2008. A composite M- With W-type of REE tetrad effect in a north China alkaline complex. *Geochim Cosmochim Acta*, 72 Supp: 11095.
- Zhao, Z. H., Z. W. Bao and Y. L. Qiao, 2010. A peculiar composite M- and W-type REE tetrad effect: evidence from the Shuiquangou alkaline syenite complex, Hebei Province, China. *Chin. Sci. Bull.* 55, 2684–2696. <https://doi.org/10.1007/s11434-010-3231-3>